Atmos. Chem. Phys., 6, 4231–4251, 2006
www.atmos-chem-phys.net/6/4231/2006/

Atmospheric Chemistry and Physics

Columnar modelling of nucleation burst evolution in the convective boundary layer – first results from a feasibility study Part III: Preliminary results on physicochemical model performance using two "clean air mass" reference scenarios

O. Hellmuth

Leibniz Institute for Tropospheric Research, Modelling Department, Permoserstrasse 15, 04318 Leipzig, Germany

Received: 1 August 2005 – Published in Atmos. Chem. Phys. Discuss.: 10 November 2005
Revised: 14 February 2006 – Accepted: 11 May 2006 – Published: 21 September 2006

Abstract. In Paper I of four papers, a revised columnar high-order model to investigate gas-aerosol-turbulence interactions in the convective boundary layer (CBL) was proposed. In Paper II, the model capability to predict first-, second- and third-order moments of meteorological variables in the CBL was demonstrated using available observational data. In the present Paper III, the high-order modelling concept is extended to sulphur and ammonia chemistry as well as to aerosol dynamics. Based on the previous CBL simulation, a feasibility study is performed using two "clean air mass" scenarios with an emission source at the ground but low aerosol background concentration. Such scenarios synoptically correspond to the advection of fresh post-frontal air in an anthropogenically influenced region. The aim is to evaluate the time-height evolution of ultrafine condensation nuclei (UCNs) and to elucidate the interactions between meteorological and physicochemical variables in a CBL column. The scenarios differ in the treatment of new particle formation (NPF), whereas homogeneous nucleation according to the classical nucleation theory (CNT) is considered. The first scenario considers nucleation of a binary system consisting of water vapour and sulphuric acid (H_2SO_4) vapour, the second one nucleation of a ternary system additionally involving ammonia (NH_3). Here, the two synthetic scenarios are discussed in detail, whereas special attention is payed to the role of turbulence in the formation of the typical UCN burst behaviour, that can often be observed in the surface layer. The intercomparison of the two scenarios reveals large differences in the evolution of the UCN number concentration in the surface layer as well as in the time-height cross-sections of first-order moments and double correlation terms. Although in both cases the occurrence of NPF bursts could be simulated, the burst characteristics and genesis of the bursts are completely different. It is demonstrated, that observations from the surface layer alone are not conclusive to elucidate the origin of newly formed particles. This is also true with respect to the interpretation of box modelling studies. The binary and ternary NPF bursts observed in the surface layer differ with respect to burst amplitude and phase. New particles simulated in the binary scenario are formed in the forenoon in the upper part of the growing CBL, followed by turbulence-induced top-down transport. Hence, with respect to the burst observation site in the surface layer, new particles are formed ex situ. In opposite to this, the ternary case reveals a much more complex pattern. Here, NPF is initiated in the early morning hours in the surface layer, when temperature (T) is low and relative humidity (RH), sulphur dioxide (SO_2) and NH_3 concentrations are high, hence new particles are formed in situ. Shortly after that, ex situ NPF in the free troposphere sets in, followed by entrainment and top-down diffusion of newly formed particles into the surface layer. Altogether, these processes mainly contribute to the formation of a strong burst in the morning hours in the ternary scenario. While the time-height cross-section of the binary nucleation rate resembles a "blob"-like evolution pattern, the ternary one resembles a "sucking tube"-like pattern. The time-height cross-sections of the flux pattern and double correlations could be plausibly interpreted in terms of CBL turbulence and entrainment/detrainment processes both in the binary and in the ternary case. Although the present approach is a pure conceptual one, it shows the feasibility to simulate gas-aerosol-turbulence interactions in

Correspondence to: O. Hellmuth
(olaf@tropos.de)

Published by Copernicus GmbH on behalf of the European Geosciences Union.

the CBL. Prior to a dedicated verification/validation study, further attempts are necessary to consider a more advanced description of the formation and activation of thermodynamically stable clusters according to modern concepts proposed by Kulmala et al. (2000), Kulmala (2003) and Kulmala et al. (2004a).

1 Introduction

Atmospheric NPF is known to frequently occur all around the world (Kulmala et al., 2004b). It is generally accepted to be a key process in regional and global climate control by aerosols, that deserves a better description in atmospheric models (Kulmala, 2003). A comprehensive review of observations and phenomenological studies of NPF, atmospheric conditions under which NPF has been observed and empirical nucleation rates etc. over the past decade from a global retrospective and from different sensor platforms was performed by Kulmala et al. (2004b). With respect to full understanding of atmospheric nucleation Kulmala (2003, p. 1001) raised two fundamental questions, which are deserved to be answered:

1. Do neutral, stable clusters exist in the atmosphere? Ion clusters do exist, but the nucleation rate predicted by the ion-mediated mechanism is limited by ion production rate, which often gives lower particles nucleation rates than observed.

2. Which mechanism governs the initial growth?

To answer these questions, Kulmala (2003) demands an interdisciplinary approach involving laboratory experiments, continuous field observations, new theories and dynamic models. With respect to the latter aspect, here an attempt is made to elucidate the possible role of CBL turbulence in NPF by means of a columnar model.

Based on the simulation of the evolution of a typical CBL, described in Paper II, in the present Paper III the physicochemical conditions of NPF in the anthropogenically influenced CBL is investigated. Within the framework of a feasibility study two exemplary scenarios are investigated to demonstrate, that the model gives reasonable results. In the present paper, special attention is payed to the interpretation of the time-height cross-sections of first- and second-order moments of physicochemical properties under turbulent conditions. The aim of the present study is to elucidate the role of turbulent diffusion and mixing in the initiation of NPF bursts, that can often be deduced from in situ aerosol measurements performed in the convective surface layer (see the generalised evolution pattern in Fig. 1 of Paper I).

Here, the NPF evolution for a homogeneous binary and ternary "clean air mass" nucleation scenario is investigated.

2 Treatment of "spurious oscillations"

In Subsubsection 5.2.1 and Section 6 of Paper I the origin of non-physical solutions, so-called spurious oscillations, of the third-order turbulence model and measures to damp them were discussed. While the addition of an artificial diffusion term to the right-hand sides of the third-order moment equations was found to efficiently damp such non-physical solutions in the meteorological part of the model, it does not in the physicochemical part. From a series of numerical experiments it was found, that in the model equations including the full physicochemical interactions, described in Appendix C2 of Paper I, spurious oscillations were already amplified and became dominant after a couple of hours of integration time until an abnormal end of the simulation. Under no circumstances it was possible to find stable solutions of the model system, when physicochemical source/sink terms (interaction of reactive tracers) were considered. The solution was found to be very sensitive against the vertical gradient of the mean physicochemical variables, $\partial\overline{\chi_\alpha}/\partial z$, α=1, ..., N, appearing in the third-order moment equations of Appendix C3 of Paper I, i.e., in the governing equations for the turbulent transport of scalar fluxes (Appendix C3.2, Eq. (C29)) and the turbulent transport of scalar correlations (Appendix C3.3, Eq. (C32) and Appendix C3.4, Eq. (C35)). To investigate its influence on the evolution of first-, second- and third-order moments a number of runs were performed, in which the original mean gradient term was adjusted by an artificial reduction factor, i.e., $(1-C_{12})\times(\partial\overline{\chi_\alpha}/\partial z)$, α=1, ..., N, with C_{12} varying between 0 (original formulation) and 1 (vanishing mean gradient). It was found, that C_{12} strongly affects the time period during which the solution remains stable. However, the only way to keep the simulation stable over the whole integration time was to set C_{12}=1. The reason for that behaviour is not yet clear. For the time being, the consideration of the reduction factor in front of the mean gradient term for the physicochemical variables is only an ad hoc approach to damp self-amplifying oscillations. However, in their high-order model Verver et al. (1997, Eq. (8), see references therein) conducted a number of similar simplifications in the governing equation of third-order moments. Among others, the authors neglected all terms of the form $M_3\partial M_1/\partial z$, where M_1 and M_3 are the averaged first and third moments, respectively: *"It is motivated by the notion that within the bulk of the unstable boundary layer the mean gradient of scalar quantities ($\partial M_1/\partial z$), as well as terms that contain this gradient, are small"* (Verver et al., 1997, pp. 200–201).

3 Parameter dependency of different nucleation mechanisms

Figure 1 shows the parameter dependency of different state-of-the-art nucleation models and parameterisations based on the CNT. Kinetic models are not considered. As seen

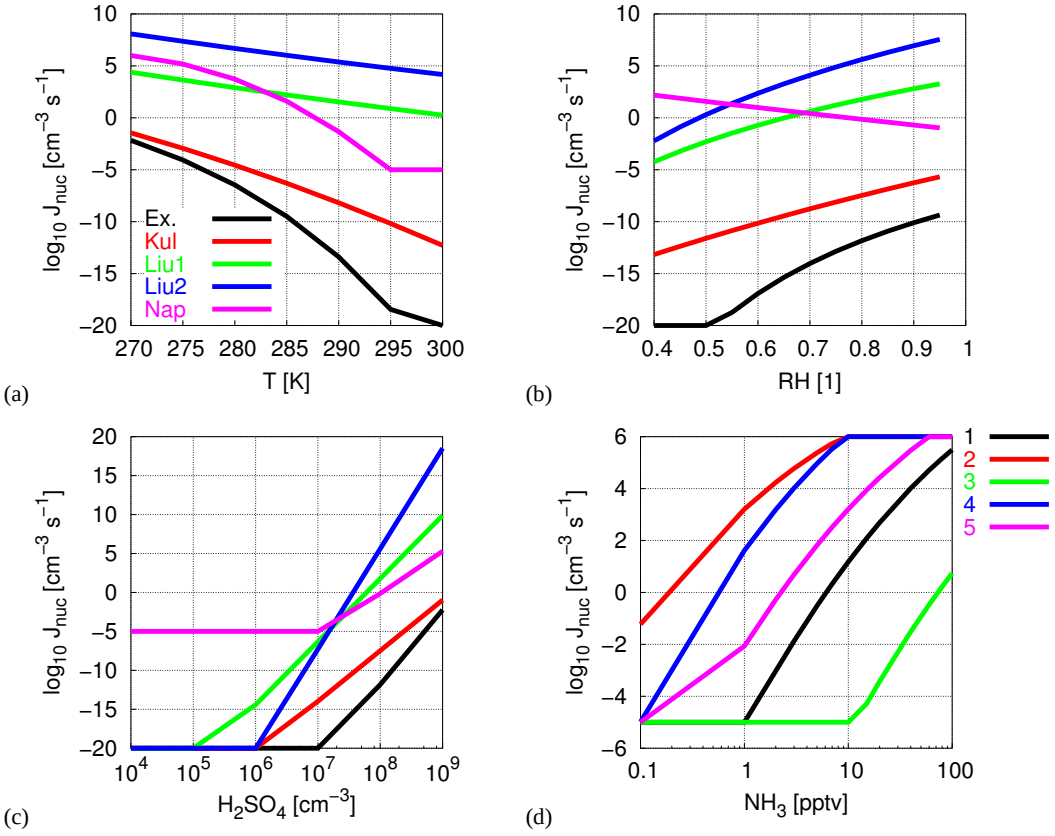

Fig. 1. Parameter dependence of different nucleation rate models: "Ex." – Exact model with consideration of cluster hydration effects (Stauffer, 1976; Jaecker-Voirol et al., 1987; Jaecker-Voirol and Mirabel, 1988, 1989; Kulmala and Laaksonen, 1990; Laaksonen and Kulmala, 1991; Kulmala et al., 1998; Seinfeld and Pandis, 1998, Chapter 10); "Kul" – Parameterisation of binary nucleation rate inclusive hydration effects according to Kulmala et al. (1998); "Liu1" – Parameterisation of binary nucleation rate according to Liu et al. (2001, Eq. (3)); "Liu2" – Parameterisation of ternary nucleation rate at an implicit NH_3 mixing ratio of 0.5 pptv according to Liu et al. (2001, Eq. (21)); "Nap" – Parameterisation of ternary nucleation rate according to Napari et al. (2002b); (a) Temperature dependence at RH=0.8, [H_2SO_4]=10^8 cm^{-3}, [NH_3]=0.5 pptv; (b) Humidity dependence at T=288.15 K, [H_2SO_4]=10^8 cm^{-3}, [NH_3]=0.5 pptv; (c) H_2SO_4 vapour dependence at T=288.15 K, RH=0.8, [NH_3]=0.5 pptv; (d) Gas phase NH_3 dependence of the ternary nucleation rate according to Napari et al. (2002b, "Nap") for different parameter combinations of temperature, relative humidity and H_2SO_4 vapour concentration (1: T=288.15 K, RH=0.8, [H_2SO_4]=10^7 cm^{-3}; 2: T=273.15 K, RH=0.8, [H_2SO_4]=10^7 cm^{-3}; 3: T=288.15 K, RH=0.8, [H_2SO_4]=10^6 cm^{-3}; 4: T=288.15 K, RH=0.8, [H_2SO_4]=10^8 cm^{-3}; 5: T=288.15 K, RH=0.4, [H_2SO_4]=10^7 cm^{-3}).

from Fig. 1a, the nucleation rate strongly increases as temperature decreases. At fixed temperature, the various nucleation rate models differ by several orders of magnitude. The parameterisations of Liu et al. (2001, Eq. (21), "Liu2") and Napari et al. (2002b, "Nap") are for ternary nucleation at NH_3=0.5 pptv. As pointed out by Liu et al. (2001), the temperature dependency of the nucleation process is poorly known, and theoretical estimates of nucleation rates are notoriously uncertain, primarily due to uncertainties in the required thermodynamic data. Therefore, the large variation between different nucleation rates is not surprising but reflects the level of process understanding and parameter knowledge. The humidity dependency is shown in Fig. 1b. For most of the considered models the nucleation rate increases when relative humidity increases, except for the ternary nucleation rate of Napari et al. (2002b, "Nap"). For the ternary case Napari et al. (2002a, Figs. 8 and 9) demonstrated, that hydration consumes free H_2SO_4 molecules to the extent, that nucleation decreases regardless of increasing humidity. This effect was found to be more pronounced at low NH_3 concentrations. At low temperatures and high trace gas concentrations the nucleation rate is less dependent on relative humidity (Napari et al., 2002a). In opposite to this, the NH_3-enhanced nucleation rate derived by Liu et al. (2001, Eq. (21),"Liu2") increases with increasing relative humidity. At RH=0.8 it is approximately five orders of magnitude larger than that of Napari et al. (2002b, "Nap"). The overall variability between the different nucleation rate models is quite large at fixed humidity. The dependency on H_2SO_4 vapour is shown in

Fig. 1c. The nucleation rate increases as the H_2SO_4 vapour concentration increases. As in the foregoing cases, the various nucleation rates differ by several orders of magnitude at fixed H_2SO_4 concentration. Figure 1d shows the dependency of the ternary nucleation rate of Napari et al. (2002b, "Nap") on the NH_3 concentration for several combinations of temperature, relative humidity and H_2SO_4 vapour concentration. In general, the ternary nucleation rate increases with increasing NH_3 concentration. Comparing graph 1 and 2 in Fig. 1d one can see, that the nucleation rate is very sensitive against the temperature. At fixed NH_3 concentration, the nucleation rate increases by approximately five orders of magnitude, when temperature decreases by 15 K. A comparison of graph 1 and 3 in Fig. 1d shows, that a decrease of the H_2SO_4 concentration by one order of magnitude reduces the nucleation rate by approximately five orders of magnitude. The hydration effect on the nucleation rate can be seen from the comparison of graph 1 and 5 in Fig. 1d. Keeping all other parameters fixed, a reduction of the relative humidity from 0.8 to 0.4 leads to an increase of the nucleation rate by approximately two orders of magnitude.

Summing up it becomes clear, that the nucleation rate model is a highly uncertain and non-linear parameter function in the present modelling approach. However, while the absolute values of the nucleation rate strongly differ from model to model, the parameter dependencies reflecting the model sensitivity do not. While the nucleation rate determines the absolute amount of newly formed particles, the parameter dependency[1] mainly affects the UCN variation in space and time. As the different nucleation rates behave similar with respect to parameter variation, the spatio-temporal variation of the UCNs is expected to be, at least, more reliable than the absolute amount of predicted new particles.

4 Model setup

To investigate NPF events in the anthropogenically influenced CBL, the meteorological simulation described in Paper II is used as a driving environment for the physicochemical evolution leading to NPF in the CBL. Figure 2 shows the initial vertical profiles of hydroxyl radical (OH), total NH_3, SO_2 and H_2SO_4 (Fig. 2a) as well as the number and mass concentrations of nucleation mode, Aitken mode and accumulation mode particles (Figs. 2b, c). The vertical decrease obeys an e-function according to a characteristic scale height. As described in Section 6 of Paper I, here two scenarios are considered with an emission source at the ground but very low background concentrations of particles, henceforth called "clean air mass" scenarios. Such situations might be synoptically relevant in anthropogenically influenced CBLs in connection with frontal air mass change and post-frontal advection of fresh polar and subpolar air.

[1] Here, the shape of the nucleation rate function is meant, i. e, its steepness, smoothness etc.

To simplify the chemical reaction system, the evolution of OH is empirically prescribed. To consider anthropogenic influences, the reservoir of SO_2 and NH_3 is permanently supplied with emissions from surface area sources. With respect to emissions, the federal state Saxony in Germany is considered as a reference region. Covering an area of 18.413 km^2, the annual emission strength amounts 200 kt/year for SO_2 and 30 kt/year for total NH_3 (gas phase plus particle phase). The corresponding average emission rates are 3.24×10^{11} molecules $cm^{-2}\,s^{-1}$ for SO_2 and 1.83×10^{11} molecules $cm^{-2}\,s^{-1}$ for total NH_3, respectively. The SO_2 emission rate is approximately 50% of that used in the urban case scenario U3 of Pirjola and Kulmala (1998, Table 2). For simplicity, the emissions were put into the surface layer at a mean emission rate.

The very low background particle concentration considered here has been chosen to simulate a very low condensation sink as a prerequisite for the availability of a high amount of the H_2SO_4 vapour to get an evaluable nucleation signal. The choice of a comparatively high pseudo-second order rate coefficient for the reaction of SO_2 with OH (see Paper I, Subsubsection 5.2.2) and a comparatively low H_2SO_4 sticking probability (see Paper I, Subsubsection 5.2.5) also moves the H_2SO_4 vapour concentration toward higher values, which can easily result in an overprediction of the available H_2SO_4 vapour concentration in comparison with observations. This may lead to acidity levels (and nucleation), that might be higher than that typically observed during atmospheric NPF events ($[H_2SO_4]\sim10^7$ cm^{-3}). From a number of preceding screening studies to get experience with the model sensitivity and to adjust the model to a nucleation regime it was found, that the nucleation signal strongly depends on the surface concentration of pre-existing particles as well as on the sticking probability. Hence, the present study can not claim to reproduce the very complex "reality" of atmospheric NPF. Especially, it can not contribute to the elucidation of the physicochemical processes at the Angstrom scale, that are responsible for atmospheric NPF at relative acidities being lower than that predicted by the CNT ($[H_2SO_4]_{CNT}\sim10^{10}$ cm^{-3}). Hence, the results are not directly comparable to atmospheric observations. However, to study gas-aerosol-turbulence interactions in the CBL from a mechanistic point of view, we think, that the approach presented here is at least justified within the framework of a conceptual study addressed to the role of CBL turbulence and to the application of the CNT.

Alternatively, one could also have considered another model setup with a higher background concentration of pre-existing particle surfaces (and/or higher H_2SO_4 sticking probability) and, consequently, lower H_2SO_4 concentration. A plausible mechanism to get an evaluable nucleation signal in the low-acidity regime is collision-controlled nucleation. Weber et al. (1996) proposed a semi-empirical expression for the collision-controlled nucleation rate, in which the stabilising effect of NH_3 onto subcritical clusters has been consid-

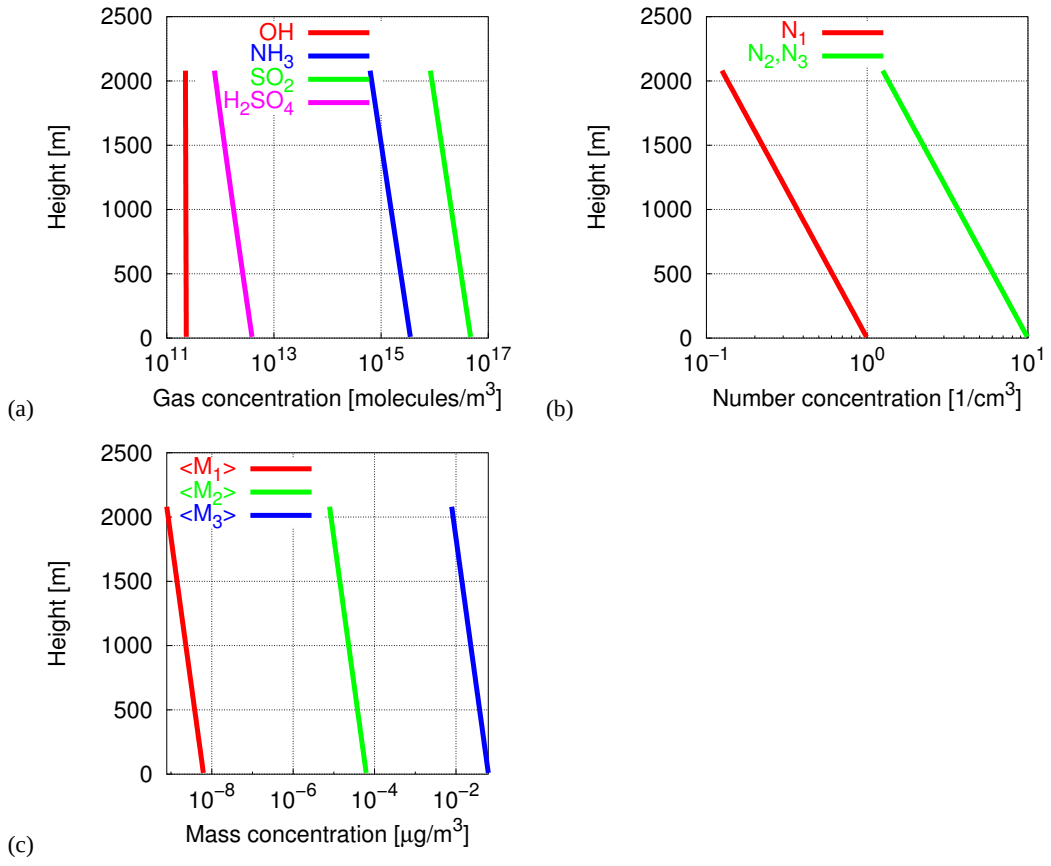

Fig. 2. Initial vertical profiles: **(a)** Gas phase concentration; **(b)** Particle number concentration; **(c)** Particle mass concentration

Table 1. Collision-controlled nucleation rate J_{obs} according to Eq. (1) (Weber et al., 1996).

H_2SO_4 [cm^{-3}]	γ=0.001	γ=0.003
1.0×10^7	0.03 cm^{-3} s^{-1}	0.27 cm^{-3} s^{-1}
5.0×10^7	0.75 cm^{-3} s^{-1}	6.75 cm^{-3} s^{-1}
1.0×10^8	3 cm^{-3} s^{-1}	27 cm^{-3} s^{-1}

ered. The steady-state rate of particle formation in the absence of cluster scavenging by pre-existing particles reads

$$J_{obs} \approx \beta\gamma^2[H_2SO_4]^2 \quad (1)$$

with $[H_2SO_4]$ being the H_2SO_4 concentration in [cm^{-3}], β=3×10^{-10} cm^3 s^{-1} being the collision frequency function for the molecular cluster, that contain the stabilised H_2SO_4 molecule, and γ being the thermodynamically determined NH_3-stabilised fraction of the H_2SO_4 monomer (γ=0.001 for Hawaii, γ=0.003 for Colorado). In Table 1, calculated nucleation rates according to Eq. (1) are shown.

From Table 1 it can be seen, that the signal from collision-controlled nucleation at $[H_2SO_4]$ $\sim10^7$ cm^{-3} is of the same order of magnitude as that obtained from the CNT presented in Fig. 4a ($J_{bin}\sim1$ cm^{-3} s^{-1}) for the high H_2SO_4 vapour concentration shown in Fig. 3e ($[H_2SO_4]_{max}$=8.8×10^9 cm^{-3}) (see Subsubsection 5.1.3). Thus, one could also study NPF within a conceptual framework like the present one at the low acidities observed in the atmosphere, when evaluating another nucleation mechanism. The question, how powerful and justified the nucleation expression given in Eq. (1) is, can not be answered here. Its investigation deserves a dedicated verification/validation study.

5 Evolution of the physicochemical variables in the CBL

5.1 First-order moments

5.1.1 OH concentration

The time-height cross-section of the photochemically driven OH concentration is presented in Fig. 3a. The evolution pattern is prescribed using an empirical relation (Liu et al., 2001) (see Paper I, Subsubsection 5.2.2, Appendix D1.1, Eq. (D2)). According to this, OH exceeds its maximum

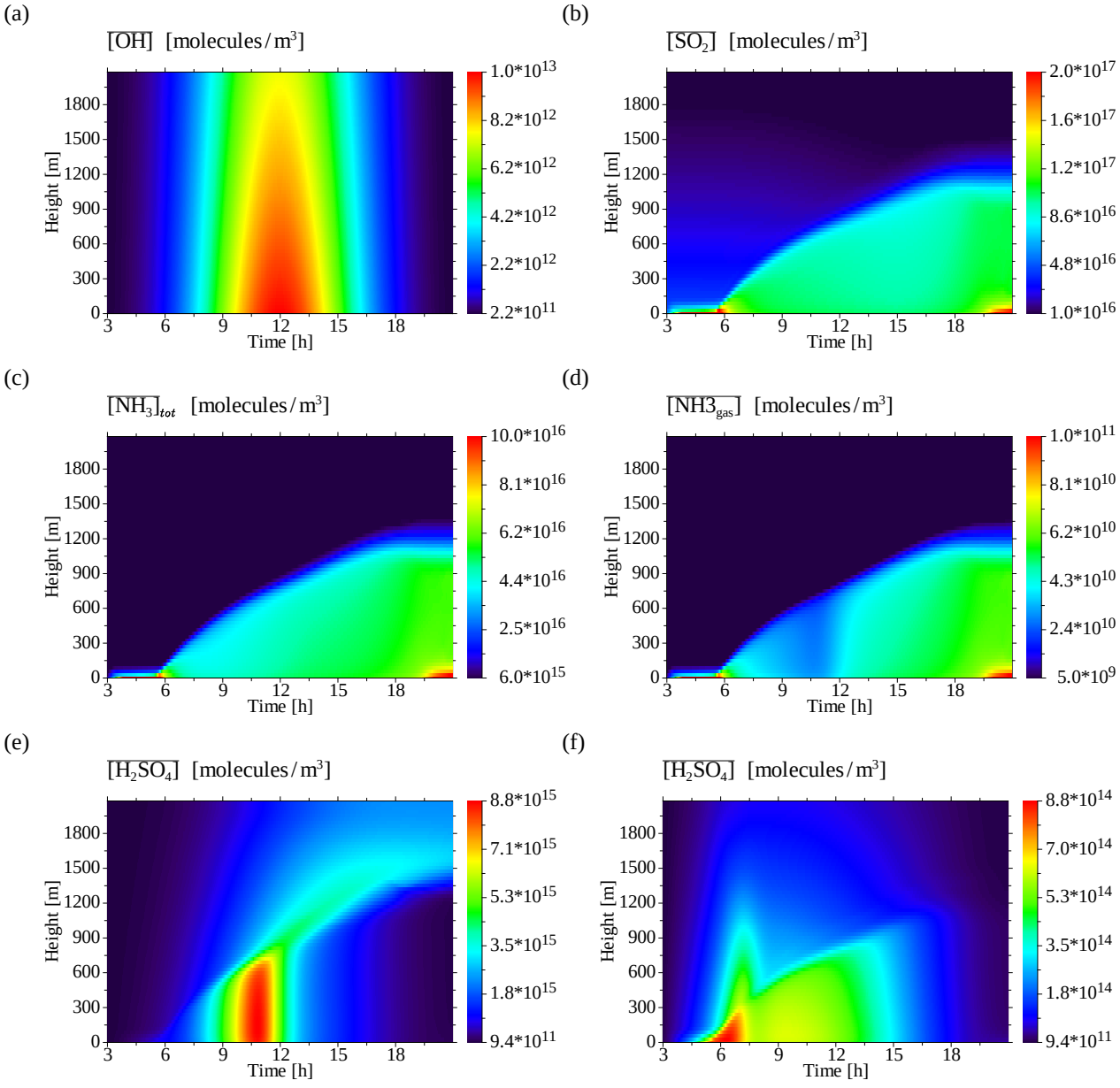

Fig. 3. First-order moments of physicochemical variables: **(a)** OH; **(b)** SO_2; **(c)** Total NH_3; **(d)** Gas phase NH_3; **(e)** H_2SO_4 – binary case; **(f)** H_2SO_4 – ternary case.

at noontime, when the solar elevation assumes its maximum. During the night, the OH concentration is hold constant at a minimum value.

5.1.2 SO_2, total NH_3 and gas phase NH_3 concentration

The evolution patterns of SO_2 (Fig. 3b), total NH_3 (Fig. 3c) and gas phase NH_3 (Fig. 3d) correspond well to the evolution of CBL turbulence. Before sunrise, turbulence is weak and only mechanically driven, which results in a very low mixing layer height (MLH). Hence, anthropogenic emissions lead to the enhancement of concentrations in the surface layer. In the course of the day, concentrations decrease due to dilution originating from buoyancy-driven turbulence. In the late afternoon turbulence weakens, afterwards a residual layer forms and near-surface concentrations increase again. The evolution of total and gas phase NH_3 proceeds nearly synchronously. The equilibrium gas phase concentration of NH_3 is approximately six orders of magnitude lower than the total NH_3 concentration.

5.1.3 H_2SO_4 concentration and nucleation rate

The evolution of H_2SO_4 vapour (Figs. 3e, f) strongly depends on the considered nucleation mechanism. Figure 3e shows the H_2SO_4 evolution in the course of the day for binary homogeneous nucleation of H_2SO_4 and water vapour. After sunrise, the H_2SO_4 concentration starts to rise due to the photooxidation of SO_2 by OH. When the H_2SO_4 concentration apparently exceeds a certain threshold value[2], noteworthy nucleation can occur, as seen from the time-height cross-section of the binary nucleation rate in Fig. 4a. The nucleation occurs in the forenoon within the growing CBL, namely just below the CBL top. The NPF event resembles a "blob"-like pattern in the time-height cross-section. According to this, new particles form in the upper third of the CBL, where temperature is low enough and relative humidity and acidity are high enough to initiate binary nucleation. In the present case, entrainment of UCNs from the residual layer or free troposphere does not contribute to the aerosol evolution, because the initial UCN concentration in the free troposphere is very low in the considered scenario. After new particles were formed and diluted within the developing CBL, the H_2SO_4 concentration decreases except for the region outside the CBL. The newly formed particles within the CBL may serve as a condensation sink for H_2SO_4 vapour, leading to a "self-cleansing" of the CBL from condensable gases. Above the CBL, this does not happen. When the H_2SO_4 concentration within the CBL apparently drops below a certain threshold, binary nucleation immediately breaks up.

The evolution of the H_2SO_4 concentration for ternary nucleation of water vapour, H_2SO_4 and NH_3 (Fig. 3f) is qualitatively and quantitatively different from that for the binary case (Fig. 3e). In the ternary case, the maximum of the H_2SO_4 concentration is one order of magnitude lower compared to the binary case. This is due to the larger condensation sink provided by newly formed particles as well as due to the nucleation loss of H_2SO_4 molecules (i.e., the number of molecules consumed in the formation of the critical embryo). Thus, the differences in the H_2SO_4 evolution originate from the different nucleation rate evolution.

The maximum H_2SO_4 concentration in the binary nucleation scenario (Fig. 3e) exceeds $[H_2SO_4]_{max}=8.8\times10^9\,cm^{-3}$. Liu et al. (2001, Fig. 2b, 8b) reported on simulated maxima of the H_2SO_4 concentrations over the Northwestern Atlantic of $[H_2SO_4]_{max}\sim2$ pptv $\approx5\times10^7\,cm^{-3}$. For a rural continental mountain site in Southern Germany (Hohenpeissenberg), Birmili et al. (2000, Fig. 1) reported on a calculated maximum of $[H_2SO_4]_{max}\sim2.5\times10^7\,cm^{-3}$ and on an observed one of $[H_2SO_4]_{max}\sim1.5\times10^7\,cm^{-3}$. Later on, Birmili et al. (2003, Fig. 7) confirmed an order of magnitude above $10^7\,cm^{-3}$ for the daily maximum H_2SO_4 concentration at the Hohenpeissenberg observatory. Based on measurements performed during the EU project QUEST (Quantification of Aerosol Nucleation in the European Boundary Layer), which was conducted in Hyytiälä, Finland in March–April 2003, Boy et al. (2005, Table 1, Fig. 8) reported on maximum midday H_2SO_4 concentrations varying between $3\times10^5-1.9\times10^7\,cm^{-3}$ for the measurements and $3\times10^5-1.4\times10^7\,cm^{-3}$ for the calculations, respectively. Measured H_2SO_4 concentrations were found to be by a factor of 1.46 higher in "polluted air masses" (originating over Central Europe or UK) than in "clean air masses" (originating over the Northern Atlantic or the polar regions). Hence, compared to this values, the H_2SO_4 concentration in the present simulations is overestimated.

The nucleation rates for both scenarios are depicted in Figs. 4a and b. In contrast to the binary nucleation rate (Fig. 4a), the ternary one (Fig. 4b) assumes its maximum at the top of the model domain. The maximum itself is three orders of magnitude higher compared to that of the binary nucleation rate. It should be noted, that the parameterisation formula for the ternary nucleation rate cannot be used to obtain the binary H_2O/H_2SO_4 vapour limit (corresponding to vanishing NH_3 concentration) or the H_2O/NH_3 limit (corresponding to vanishing H_2SO_4 concentration). This results from the fact, that the natural logarithm, being a part of the parameterisation of the ternary nucleation rate, is infinite for argument zero (i.e., for vanishing concentrations) (Napari et al., 2002b). The nucleation rate maximum at the top of the model domain reflects the temperature dependency of the nucleation rate parameterisation at the ambient H_2SO_4 and gas phase NH_3 concentration there, but to a higher extent the humidity dependency of the ternary nucleation rate. As seen from Korhonen et al. (1999, Figs. 2 and 3), Napari et al. (2002a, Figs. 8 and 9) and Napari et al. (2002b, Fig. 4), the ternary nucleation rate strongly increases with decreasing relative humidity at constant temperature and acidity. Napari et al. (2002a, p. 4226) wrote: "[...] *nucleation rate decreases with increasing water content in the vapour. However, the constant free* H_2SO_4 *curves show the expected upward slope, which indicates that hydration consumes free* H_2SO_4 *to the extent, that nucleation slows regardless of increasing* RH*. This effect is more pronounced at low* NH_3 *concentrations. Nucleation rate seems to be less dependent on* RH *at low temperatures and high trace gas concentrations, which is not surprising since the corresponding critical clusters are almost water-free.*" The authors emphasised, that their old model for ternary nucleation suggested, that the nucleation rate is almost independent on RH. Considering the time-height evolution of the relative humidity presented in Fig. 3f of Paper II, it appears, that the relative humidity attains its minimum ($RH_{min}\sim10\%$) at the top of the model domain according to the chosen model setup. Hence, the simulated maximum of the ternary nucleation rate at the top of the model domain is reasonable.

The pattern of the H_2SO_4 evolution in the ternary case results from superposition of photochemical activity and CBL turbulence. In the early morning, the H_2SO_4 concentration

[2] Based on visual inspection.

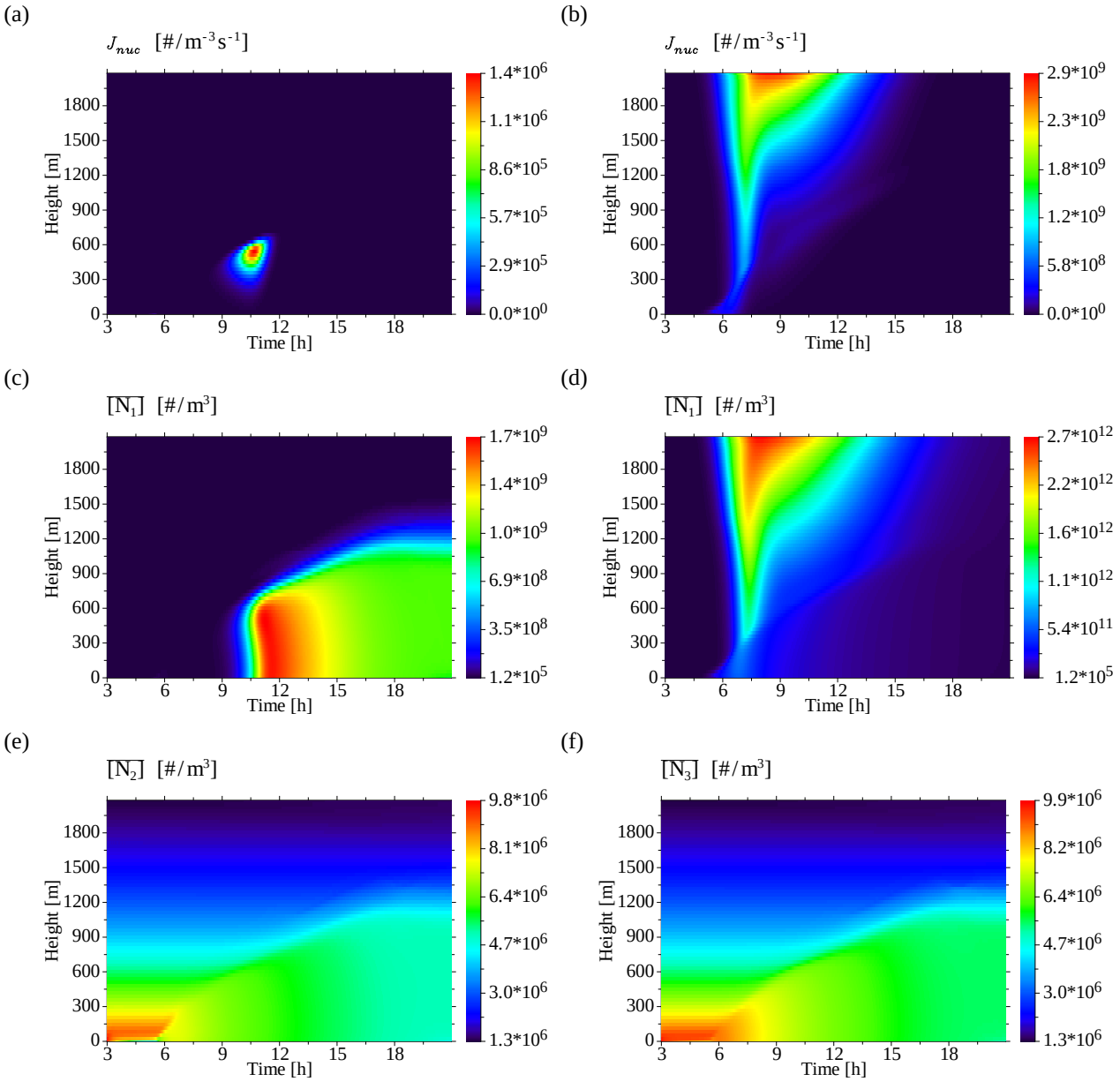

Fig. 4. First-order moments of physicochemical variables: **(a)** Binary nucleation rate; **(b)** Ternary nucleation rate; **(c)** UCN number concentration – binary case; **(d)** UCN number concentration – ternary case; **(e)** Aitken mode number concentration – binary case; **(f)** Accumulation mode number concentration – binary case.

increases due to photooxidation of SO_2 after sunrise. As the MLH limits the vertical extension of the diffusion domain, SO_2 concentration is enhanced below the MLH due to anthropogenic emissions. Hence, the H_2SO_4 concentration is elevated too. Above the MLH, the formation of H_2SO_4 is limited by the given background SO_2 concentration, which is set up by the initial profile of SO_2. Therefore, the H_2SO_4 formation above the MLH is lower than that in the mixing layer. Due to the low temperature and humidity at the top of the model domain, the nucleation rate forms a "virga"-like pattern in the time-height cross-section (Fig. 4b), resembling a "sucking tube". The ternary nucleation rate strongly decreases from the top of the model domain toward the surface layer. However, in the course of the day the nucleation starts in the surface layer but not at the top of the model domain. In the surface layer, the temperature is in fact higher compared to that at the top of model domain, hence reducing the nucleation rate. But this damping effect is overcompensated by the enhanced near-surface concentration of NH_3 and H_2SO_4 vapour. Thus, new particles form at a low rate. Later on, when H_2SO_4 formation increases with the rising sun, the nucleation maximum moves toward the region with lower tem-

peratures, i.e., toward higher levels. Here, nucleation occurs at much higher rates. In this way, the early start of nucleation in the surface layer and the delayed NPF burst originating above the MLH are mainly an effect of the non-linearity and the varying sensitivity of the nucleation rate throughout the input parameter space.

When UCNs have been formed, the further evolution of H_2SO_4 vapour is controlled by condensation growth. As the bulk of particles is formed above the MLH, the condensation growth is also larger there. In the mixing layer, the H_2SO_4 concentration is mainly influenced by turbulent dilution. The decrease of H_2SO_4 concentration within the CBL in the afternoon corresponds to the cumulative condensation sink there. It should be noted, that the maximum of H_2SO_4 concentration in the ternary case is one order of magnitude lower than that in the binary case. This corresponds to the much higher condensation sink in the ternary case, resulting from nucleation at much higher rates.

The strong nucleation signal in the binary scenario is a consequence of the overprediction of the H_2SO_4 concentration in the present simulation, which nearly exceeds the required threshold of $\sim 10^{10}\,cm^{-3}$ predicted by the CNT. Nevertheless, the characteristics and diurnal variation can be studied by means of the considered scenarios.

5.1.4 Particle number concentration

The evolution patterns of the particle number concentration are presented in Figs. 4c–f. The time-hight cross-sections of the UCN number concentration[3] for the binary case (Fig. 4c) and for the ternary one (Fig. 4d) correspond well to those for the considered nucleation rates (Figs. 4a and b, respectively).

At first, due to higher efficiency of ternary nucleation the maximum UCN number concentration for the ternary case is three orders of magnitude higher than that for the binary one. Secondly, in the binary case there appears a well-defined burst pattern in the forenoon, characterised by a strong increase between 09:00 and 11:00 Local Standard Time (LST), reaching the maximum around noon, followed by a retarded decrease afterwards. The burst is initiated by the "blob"-like NPF event (Fig. 4a) just below the top of the growing CBL. Afterwards, newly formed particles were transported downward to the surface layer by CBL turbulence. During the transport, newly formed particles were diluted and well-mixed throughout the CBL column. Once UCNs were formed, the UCN number concentration immediately begins to decrease due to intra-mode and inter-mode coagulation and deposition.

In the ternary case, the time-height evolution of UCN number concentration (Fig. 4d) corresponds also quite well to the associated nucleation pattern. In the surface layer, the UCN number concentration starts to rise immediately after sunrise due to in situ ternary nucleation. Following the "sucking tube"-like evolution pattern of the ternary nucleation rate (Fig. 4b), the UCN number concentration assumes a temporally broadened maximum at the top of the model domain in the forenoon. From there, the UCN number concentration decreases toward the CBL. Once captured by entrainment processes, newly formed particles enter the CBL, where they were diluted and well-mixed. Downward diffusion of entrained UCNs enhances the UCN number concentration in the surface layer. According to this scenario, NPF starts in situ in the surface layer in the early morning, afterwards enhanced by downward transport of entrained UCNs. Outside the CBL, the UCN number concentration pattern is not blurred, because turbulent diffusion is small there. As for the binary case, the UCN concentration decreases within the CBL in the course of the day by intra-mode and inter-mode coagulation and deposition.

The time-height evolution patterns of the number concentration of the Aitken mode (Fig. 4e) and accumulation mode particles (Fig. 4f) for binary nucleation are nearly identical to those for ternary one (not shown). This is plausible, because coagulation with UCNs does not change the number concentration of pre-existing Aitken mode and accumulation mode particles. The particle number in the corresponding larger modes is conserved when larger particles collide with smaller ones. The time-height cross-sections of the respective particle number concentrations correspond well to the CBL evolution. At the initial state, the number concentrations of pre-existing Aitken mode and accumulation mode particles decrease with height. In the surface layer, the Aitken mode number concentration already decreases due to deposition at night-time. Because of the particle size dependency of the deposition velocity, deposition of accumulation mode particles is much smaller. When turbulence set in, the pre-existing Aitken mode and accumulation mode particles are diluted throughout the mixing layer, leading to well-mixed vertical distributions. The temporal decrease of the particle number concentration in both modes is due to intra-mode and inter-mode coagulation. The impact of the particle radius onto the coagulation coefficient results in only very small differences in the coagulation loss between the binary and the ternary case. The particle radius is diagnostically determined from particle number and mass concentration. For Aitken mode particles, the coagulation loss is slightly enhanced for the ternary case compared to the binary one. However, for accumulation mode particles there are no observable differences between the evolution patterns of the binary and ternary case, respectively.

[3] As only mass and number concentration are predictive variables, the UCN size range is diagnostically determined. It is calculated from the corresponding mode number and mass concentration after each integration time step. At the initial state, the particle radii are $r_{0,1}=1\times10^{-9}$ m for the UCN mode, $r_{0,2}=10\times10^{-9}$ m for the Aitken mode, $r_{0,3}=100\times10^{-9}$ m for the accumulation mode.

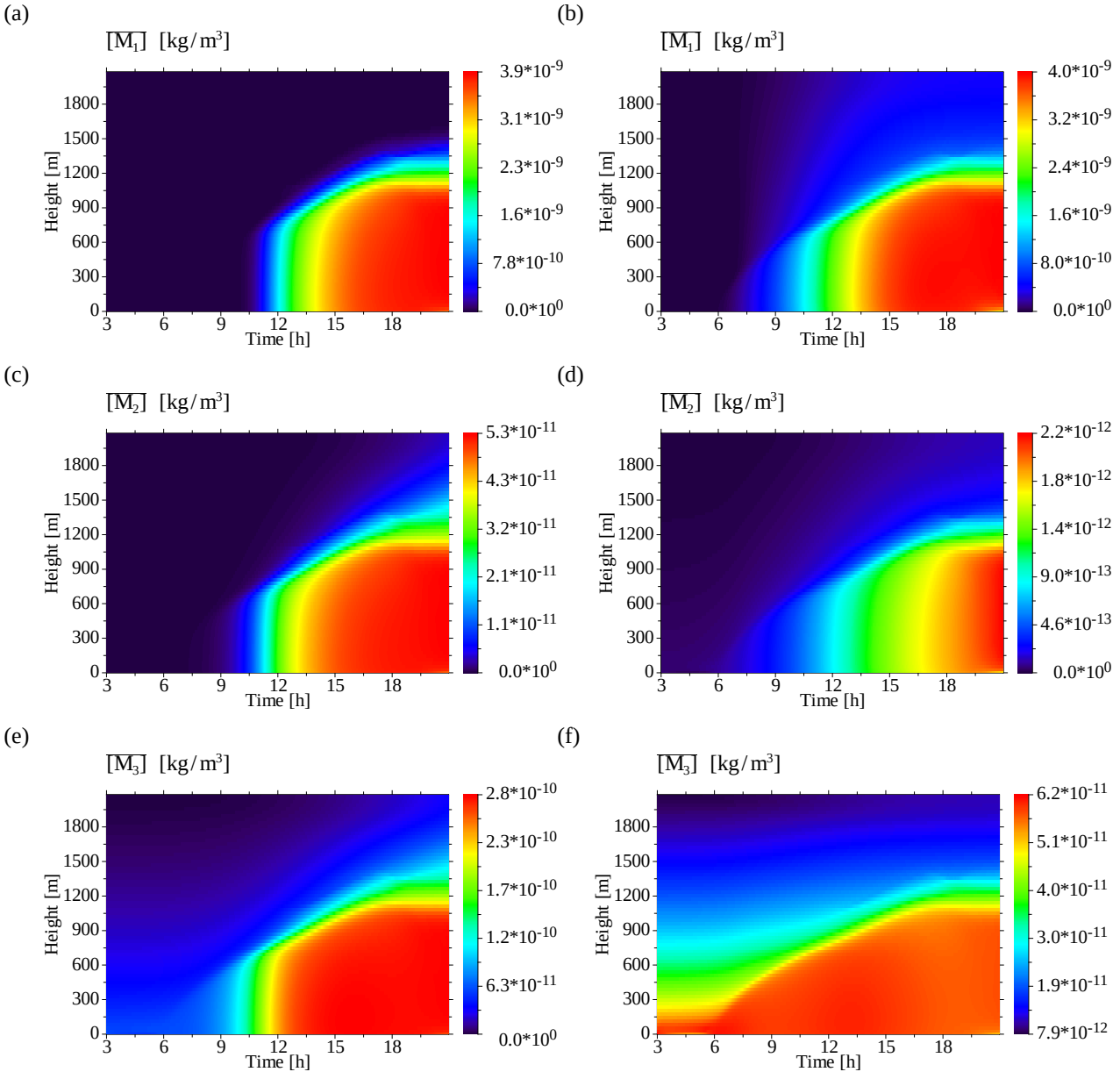

Fig. 5. First-order moments of physicochemical variables: **(a)** UCN mass concentration – binary case; **(b)** UCN mass concentration – ternary case; **(c)** Aitken mode mass concentration – binary case; **(d)** Aitken mode mass concentration – ternary case; **(e)** Accumulation mode mass concentration – binary case; **(f)** Accumulation mode mass concentration – ternary case.

5.1.5 Particle mass concentration

The evolution patterns of the mass concentration are depicted in Figs. 5a–f.

The mass concentrations of UCN mode, Aitken mode and accumulation mode particles significantly differ for binary and ternary nucleation, respectively. The time-height cross-section of the UCN mass concentration in the binary case (Fig. 5a) corresponds well to the pattern of the H_2SO_4 concentration (Fig. 3e) and the UCN number concentration (Fig. 4c). A significant gain of particle mass by H_2SO_4 condensation can be firstly observed after UCN number concentration has exceeded its maximum. Hence, the temporal progression of cleansing the CBL from condensable H_2SO_4 vapour for binary nucleation might be thought as follows:

1. Increase of the OH concentration after sunrise;

2. Initiation of H_2SO_4 production with subsequent exceedance of a critical H_2SO_4 vapour threshold;

3. Onset of an elevated "blob"-like nucleation burst just below the top of the developing CBL, followed by turbulence-induced downward transport of UCNs, which leads to a well-mixed vertical UCN profile;
4. Subsequent increase of the UCN number concentration throughout the CBL until a certain level for initiation of condensation growth has been reached;
5. Onset of significant UCN mass accumulation due to H_2SO_4 condensation throughout the entire CBL;
6. Decrease of the UCN number concentration due to intra-mode and inter-mode coagulation, decrease of the H_2SO_4 vapour concentration due to deposition loss of vapour molecules onto newly formed particles, pre-existing Aitken mode and accumulation mode particles, leading to a cleansing of the CBL from condensable vapours.

For the ternary case, the evolution pattern of UCN mass concentration (Fig. 5b) is qualitatively similar to that for the binary case (Fig. 5a), except for the start-up phase of condensation growth. The difference between the daytime maxima of the UCN mass concentrations is small. However, due to in situ ternary nucleation occurring in the surface layer in the early morning, a much higher UCN number concentration compared to the binary case is available to serve as a condensation sink at that time. Hence, mass accumulation by H_2SO_4 condensation growth can start earlier. Owing to the formation of new particles above the CBL, mass accumulation occurs also there. Nonetheless, the mass accumulation within the CBL exceeds that in the free troposphere, since much more condensable vapour is available within the CBL, which originates from low-level emission of the precursor gas SO_2 and subsequent photooxidation to produce H_2SO_4 vapour. CBL turbulence ensures, that condensation sinks and condensable vapour are well-mixed throughout the CBL, hence vertically homogenising the UCN mass distribution within the mixing layer.

The differences in the UCN number concentrations for the binary and ternary case, respectively, lead to corresponding differences in the mass concentrations of pre-existing Aitken mode (cf. Figs. 5c, d) and accumulation mode particles (cf. Figs. 5e, f). Aitken mode particles serve as a coagulation sink for UCNs and as a deposition sink for H_2SO_4 vapour. Accumulation mode particles serve as a coagulation sink for both UCNs and Aitken mode particles and as a deposition sink for H_2SO_4 vapour. Hence, differences in UCN number concentration propagate upward across the mode cascade to affect the larger size modes, i.e., changes in UCN number concentration influence the Aitken and accumulation mode, even small[4].

This can be seen in the mass concentrations of the Aitken mode and accumulation mode particles. In the ternary case, the maximum mass concentration of both modes is somewhat lower compared to the corresponding binary cases. This can be explained by the lower supply with condensable vapour in the ternary case (see H_2SO_4 concentration in Figs. 3e, f), originating from larger nucleation loss of H_2SO_4 molecules to form a critical embryo. In the ternary case, more H_2SO_4 molecules are consumed in the formation of new embryos rather than condensed onto the pre-existing particle surface. We must remember, that the number concentration of pre-existing particles was chosen to be very low at the initial state. The net accumulation of H_2SO_4 vapour in these modes competes with that in the UCN mode, and uncertainties in the H_2SO_4 vapour evolution may become crucial in the mass balance of the pre-existing particles. Anyway, the main difference between the time-height evolution of the Aitken mode and accumulation mode concentration of the binary and the ternary case, respectively, consists in the earlier begin of the mass accumulation. The explanation of the quantitative differences deserves further investigations.

5.2 Second-order moments

5.2.1 Remarks

From the large number of predictive second-order moments only those are depicted, which can be interpreted with respect to NPF events in the CBL. In opposite to the meteorological variables, empirical findings on second-order moments of physicochemical variables are still very rare. However, the simulation results will be compared with previous findings as far as possible.

5.2.2 Turbulent vertical flux

Although not possible to be verified by observations, the turbulent vertical flux of total NH_3 (Fig. 6a) and SO_2 (Fig. 6b) corresponds well to the flux pattern of non-reactive scalars expectable in the CBL. In both cases, the flux is always positive within the CBL in the course of the day except for the lowest half-level, where it becomes negative owing to dry deposition. The turbulent transport is upward directed, because the chemical species were released into the surface layer. Hence, the concentrations of the species decrease with height.

The vertical flux pattern of the pseudo-reactive H_2SO_4 vapour is much more complicated and reveals strong differences between the binary (Fig. 6c) and the ternary case

[4]Example: Assuming some non-linear dependency $y_j = f_j(x_i)$ between a set of dependent variables y_j, $j=1, \ldots, N$ and a set of independent variables x_i, $i=1, \ldots, n$. Then, the change of y_j due to variations in x_i can be approximated according to the law of error propagation, i.e., $\Delta y_j \approx \sum_i^n (\partial f_j / \partial x_i) \Delta x_i$. Here, Δy_j are the differences in y_j resulting from differences ("errors") in x_i. The sensitivity of y_j against x_i depends on the first partial derivatives $\partial f_j / \partial x_i$.

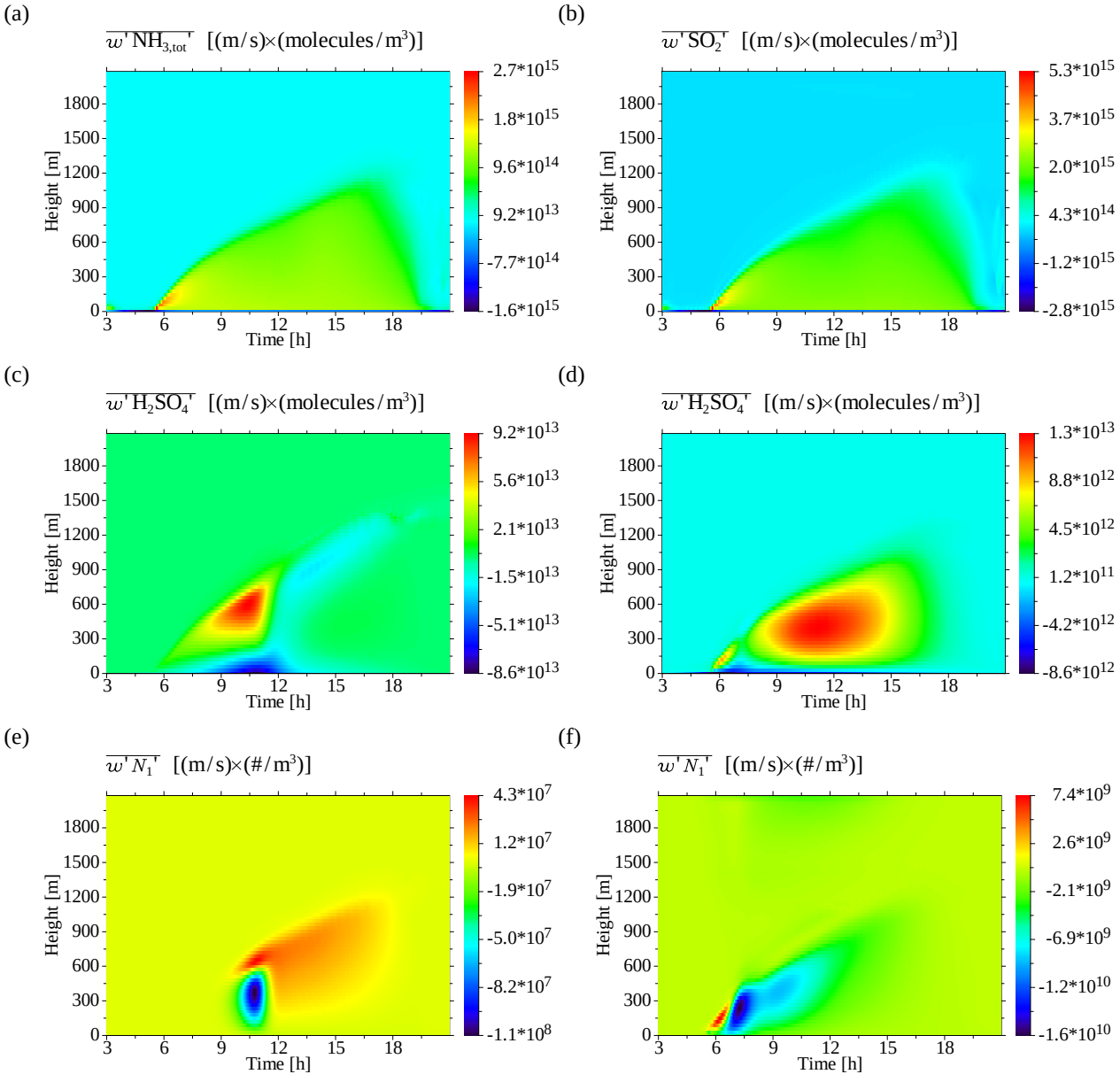

Fig. 6. Turbulent vertical fluxes of physicochemical species: **(a)** Total NH_3 flux; **(b)** SO_2 flux; **(c)** H_2SO_4 flux – binary case; **(d)** H_2SO_4 flux – ternary case; **(e)** UCN number concentration flux – binary case; **(f)** UCN number concentration flux – ternary case.

(Fig. 6d). In the binary case, the initial vertical flux is zero at all heights. When CBL turbulence sets in, the vertical flux becomes greater zero, indicating a weak upward transport of H_2SO_4 vapour. Later on, when CBL turbulence intensifies, a shallow layer of downward directed turbulent flux forms in the lowest model layers while above the positive flux strengthens. Between 09:00 and 12:00 LST, the photochemically produced H_2SO_4 vapour concentration exceeds its maximum and shows a well-mixed vertical distribution throughout the CBL. The occurrence of the positive flux maximum spatio-temporally coincides with the "blob"-like binary nucleation event (Figs. 4a, c). The level of "zero flux" represents the location of an "apparent pseudo-reaction source" (net source), from which H_2SO_4 vapour is upward and downward diluted by turbulence. The vertical flux of H_2SO_4 vapour weakens, when condensation and "self-cleansing" of the CBL set in. In the late afternoon, a secondary positive flux maximum forms. We keep in mind, that the flux evolution of H_2SO_4 vapour is not only affected by turbulent diffusion, but also by higher-order moments, resulting from physicochemical interaction terms in the governing equations.

For the ternary case, the evolution pattern of H_2SO_4 vapour flux (Fig. 6d) quantitatively differs from that for the binary one, but the basic features qualitatively agree. When ternary nucleation starts in the early morning in the surface layer, a similar vertical downward/upward flux pattern as in the binary case appears there, but at a smaller time and spatial scale. This supports the assumption, that the vertical flux layering is strongly related to the nucleation loss of H_2SO_4 molecules. In opposite to the binary case, the vertical flux evolves later on toward a primary positive maximum throughout the CBL, except for the surface layer. While in the binary case the vertical flux suddenly decreases, when condensation loss of H_2SO_4 vapour onto particles becomes important, in the ternary case it does not. This is due to the lower impact of condensation loss onto newly formed particles in the CBL of the ternary case. In the ternary case, new particles were mainly formed above the CBL.
Hence, the evolution pattern of the H_2SO_4 vapour flux can be generalised as follows:

1. Appearance of a vertical two-layer H_2SO_4 flux pattern (downward/upward flux) in the pre-nucleation phase and during the NPF event;
2. Occurrence of a subsequent upward directed H_2SO_4 vapour flux in the post-nucleation phase, when condensation growth dominates.

The absolute values of the vertical flux as well as the extension and spatio-temporal distribution of the flux minima and maxima in the evolution pattern are strongly affected by physicochemical interactions, which are related to nucleation and condensation loss of H_2SO_4 vapour molecules. These interactions, represented by additional correlation terms, are usually neglected in diagnostic downgradient-flux parameterisations. A comparison with the plain structure of the time-height cross-sections of NH_3 (Fig. 6a) and SO_2 (Fig. 6b) shows, that the additional correlation terms, resulting from the gas-aerosol-turbulence interaction and appearing in the governing equation of the H_2SO_4 flux, may have a significant impact on the flux evolution. This happens especially, when highly non-linear processes such as nucleation and condensation are involved. For the time being, a direct verification of the flux of H_2SO_4 vapour is not possible due to lack of corresponding observational data. It should be noted, that the vertical profiling of H_2SO_4 vapour concentrations in the CBL is hard to realise, especially the measurement of highly resolved spatio-temporal data series of that precursor gas to derive flux profiles. Perhaps, the present modelling approach provides some motivation for future studies to determine high-order moments, involving physicochemical species from in situ measurements and/or remote sensing.

The time-height evolution patterns of the turbulent vertical flux of the UCN number concentration for the binary case (Fig. 6e) and for the ternary one (Fig. 6f) are closely correlated to the corresponding evolution patterns of the nucleation rates (Figs. 4a, b) and the UCN number concentrations (Figs. 4c, d). In the binary case, the location of the "zero UCN flux" level coincides well in time and space with the "blob"-like source of newly formed particles (Fig. 4a). From there, the bulk of UCNs is transported downward ($\overline{w'N_1'}<0$), a certain part is transported upward ($\overline{w'N_1'}>0$) and diluted throughout the entrainment layer. It will be shown below, that this downward directed flux leads to a sudden enhancement of the UCN number concentration in the surface layer, representing the "NPF burst" in a closer sense. According to the binary scenario conceived here, this burst does not originate from in situ nucleation within the surface layer. It can be ascribed to downward transport of UCNs, recently formed in the upper third of the forenoon CBL.
In the ternary case, the flux pattern (Fig. 6f) reflects the evolution of the NPF event (Figs. 4b, d) very good. Here, the above-described downward/upward flux layering occurs in the early morning, when the CBL just starts to rise. Hence, the downward flux is restricted to occur in the lowest model layers, i.e., at lower time and spatial scales. Once in situ formed there, UCNs are immediately transported downward to the surface and upward to the entrainment layer by the developing CBL turbulence. This flux pattern corresponds well to that in the binary case, except for its smaller time and spatial scale. Shortly after initial NPF at low levels, the lower end of the "sucking tube"-like NPF pattern above the CBL merges with the preceding in situ nucleation event. The subsequent downward transport of UCNs, continuing during the forenoon, reflects the dilution of entrained UCNs from above. The absolute minimum of the UCN flux (corresponding to the absolute maximum of the downward directed flux) appears, when the UCN "sucking tube" enters the MLH and it is captured by CBL turbulence. Afterwards, the downward flux decreases with the decreasing number concentration of entrained UCNs. Supposed, that the time-height evolution of the UCN formation rate is appropriately represented by the parameterisation of the ternary nucleation rate, the vertical UCN flux pattern in Fig. 6f consistently behaves with respect to CBL turbulence and to the evolution of the UCN number concentration. Apart from the pattern differences, the absolute value of the UCN flux for the ternary case is by several orders of magnitude larger than that for the binary case. While CBL turbulence is identical in both cases, the turbulent vertical flux of UCN number concentration is higher for the ternary case.

5.2.3 Cross-correlations

$\overline{\theta' NH_{3,tot}'}$ (Fig. 7a): In the entrainment layer the potential temperature and the total NH_3 concentration are anti-correlated ($\overline{\theta' NH_{3,tot}'}<0$), indicating entrainment of potentially warmer but NH_3-depleted free-tropospheric air into the CBL and/or detrainment of potentially colder but NH_3-enriched CBL air into the free troposphere.

$\overline{q' NH_{3,tot}'}$ (Fig. 7b): The water vapour mixing ratio and the total NH_3 concentration are positively correlated in the entrainment layer ($\overline{q' NH_{3,tot}'}>0$), resulting from entrainment of drier and NH_3-depleted free-tropospheric air into the CBL and/or detrainment of moister and NH_3-enriched CBL air into the free troposphere.

$\overline{\theta' H_2SO_4'}$ (Figs. 7c, d): The correlation patterns of potential temperature and H_2SO_4 vapour for the binary and ternary case are very different. In the binary case, the correlation in the entrainment layer changes its sign in the course of the day (Fig. 7c). In the forenoon, H_2SO_4 vapour is photochemically produced in the CBL, exceeding its maximum there (Fig. 3e). Hence, during the oxidation time, turbulence causes entrainment of potentially warmer but H_2SO_4 vapour-depleted free-tropospheric air and/or detrainment of potentially colder but H_2SO_4 vapour-enriched CBL air into the free troposphere ($\overline{\theta' H_2SO_4'}<0$). Later on, after nucleation had occurred, condensation sink becomes more and more important, leading to a decrease of H_2SO_4 vapour within the CBL. Above the CBL, the UCN concentration and the condensation sink for H_2SO_4 vapour are quite low. As a result, the H_2SO_4 vapour concentration in the free troposphere is slightly higher compared to that in the CBL. Under such circumstances, turbulence leads to the entrainment of potentially warmer and H_2SO_4 vapour-enriched free-tropospheric air into the CBL and/or detrainment of potentially colder and H_2SO_4 vapour-depleted CBL air into the free troposphere ($\overline{\theta' H_2SO_4'}>0$). Thus, the time, when the cross-correlation changes its sign during the day, indicates the moment, when the H_2SO_4 vapour condensation sink becomes important. In the ternary case, the corresponding correlation in the entrainment layer remains negative during the day, showing a well-distinct absolute minimum in the early morning, which is separated from a second, more extended one lasting from the forenoon until the afternoon (Fig. 7d). The zone of anti-correlation is related to the entrainment of potentially warmer but H_2SO_4 vapour-depleted free-tropospheric air into the CBL and/or to detrainment of potentially colder but H_2SO_4 vapour-enriched CBL air into the free troposphere. As the ternary nucleation exceeds its maximum outside the CBL, the H_2SO_4 vapour condensation sink assumes its maximum also there. Hence, the H_2SO_4 vapour concentration in the CBL remains always higher than in the free troposphere (Fig. 3f). The transition between the two pronounced anti-correlation periods, appearing at around 07:00 LST, marks the temporal crossover from in situ NPF in the morning surface layer to the forenoon entrainment of UCNs, recently formed above the CBL and downward transported from there. At the crossover time, H_2SO_4 vapour condensation sink becomes important, leading to a decrease of H_2SO_4 vapour concentration. Shortly after the "sucking tube" of the UCN pattern (Fig. 4d) has entered the surface layer from above, the H_2SO_4 vapour concentration increases again.

$\overline{q' H_2SO_4'}$ (Figs. 7e, f): The correlation of water vapour mixing ratio and H_2SO_4 vapour corresponds very well to the $\overline{\theta' H_2SO_4'}$ pattern. Considering, that potential temperature and water vapour mixing ratio are anti-correlated throughout the entrainment layer, the "quasi-reversed" behaviour of the corresponding pattern pairs Figs. 7c, e and Figs. 7d, f is self-evident.

$\overline{\theta' N_1'}$ (Figs. 8a, b): The evolution patterns of the cross-correlation of potential temperature and UCN number concentration for the binary and ternary case are quite different. For binary nucleation, the potential temperature and UCN number concentration are anti-correlated in the entrainment layer (Fig. 8a), i.e., low potential temperature favours the occurrence of UCNs. The location and time of occurrence of the absolute minimum of $\overline{\theta' N_1'}$ coincide with the NPF event. This reflects the dependency of the nucleation rate on temperature. More importantly, the positive correlation within the entrainment layer during the day indicates detrainment of potentially colder but UCN-enriched CBL air into the free troposphere and/or entrainment of potentially warmer but UCN-depleted free-tropospheric air into the CBL. For the ternary case, the absolute minimum of $\overline{\theta' N_1'}$ in the early morning corresponds well to the low-level in situ formation of NPF (Fig. 8b). The subsequent positive correlation of potential temperature and UCN number concentration reflects the entrainment of potential warmer and UCN-enriched residual layer air into the CBL, the latter resulting from ternary nucleation above.

$\overline{q' N_1'}$ (Figs. 8c, d): For the binary case, the water vapour mixing ratio is positively correlated with the UCN number concentration in the entrainment layer (Fig. 8c). This behaviour is inverse to the $\overline{\theta' N_1'}$ correlation pattern (Fig. 8a) and can be partially ascribed to the enhancement of nucleation due to increased humidity. But mainly, the concurrence of the positive correlation with the entrainment layer indicates entrainment of drier and UCN-depleted free-tropospheric air into the CBL and/or detrainment of moister and UCN-enriched CBL air into the free troposphere. The inverse behaviour of the correlation patterns appearing in the $\overline{\theta' N_1'}$ and $\overline{q' N_1'}$ time-height cross-sections of the binary case can be seen also in the ternary case (Figs. 8b, d). In the early morning, the water vapour mixing ratio is positively correlated with the UCN number concentration (Fig. 8d), showing prefer-

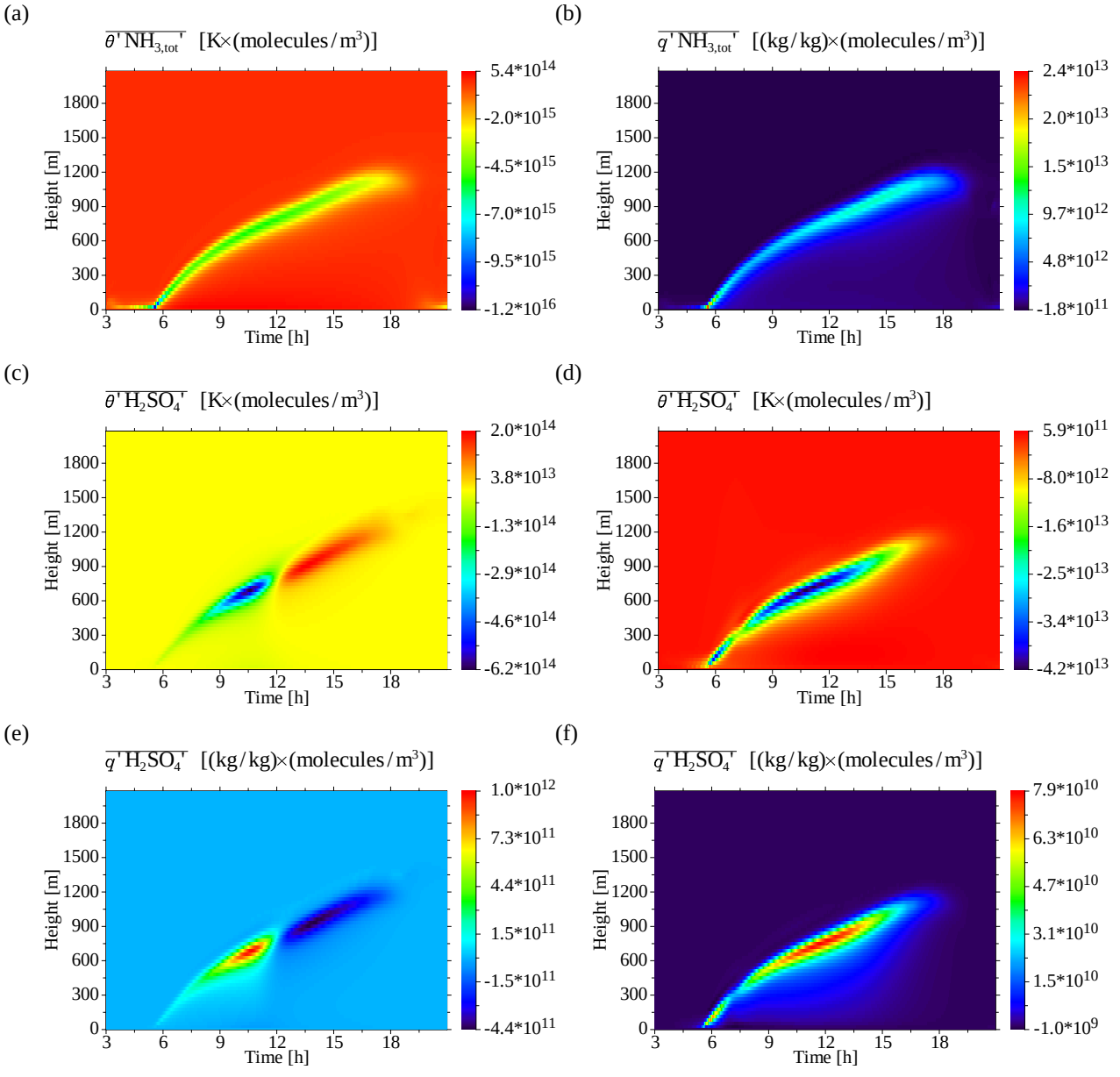

Fig. 7. Co-variances of meteorological parameters and physicochemical properties: **(a)** Co-variance of potential temperature and total NH_3 concentration; **(b)** Co-variance of water vapour mixing ratio and total NH_3 concentration; **(c)** Co-variance of potential temperature and H_2SO_4 concentration – binary case; **(d)** Co-variance of potential temperature and H_2SO_4 concentration – ternary case; **(e)** Co-variance of water vapour mixing ratio and H_2SO_4 concentration – binary case; **(f)** Co-variance of water vapour mixing ratio and H_2SO_4 concentration – ternary case.

ence of ternary nucleation due to enhanced humidity at that time. Later on, entrainment of drier but UCN-enriched free-tropospheric air becomes dominant, leading to $\overline{q' N_1'} < 0$ in the entrainment layer. Hence, the $\overline{\theta' N_1'}$ and $\overline{q' N_1'}$ evolution patterns are consistent with the evolution of CBL turbulence and the supposed nucleation mechanism.

$\overline{NH_{3,tot}' N_1'}$ (Figs. 9a, b): The cross-correlations of total NH_3 and UCN number concentration strongly differ between the binary and ternary case. In the binary case, the total NH_3 concentration is positively correlated with UCN number concentration in the entrainment layer after nucleation has occurred. This positive correlation in the late forenoon indicates detrainment of total NH_3 and UCN-enriched CBL air into the free troposphere and/or entrainment of free-

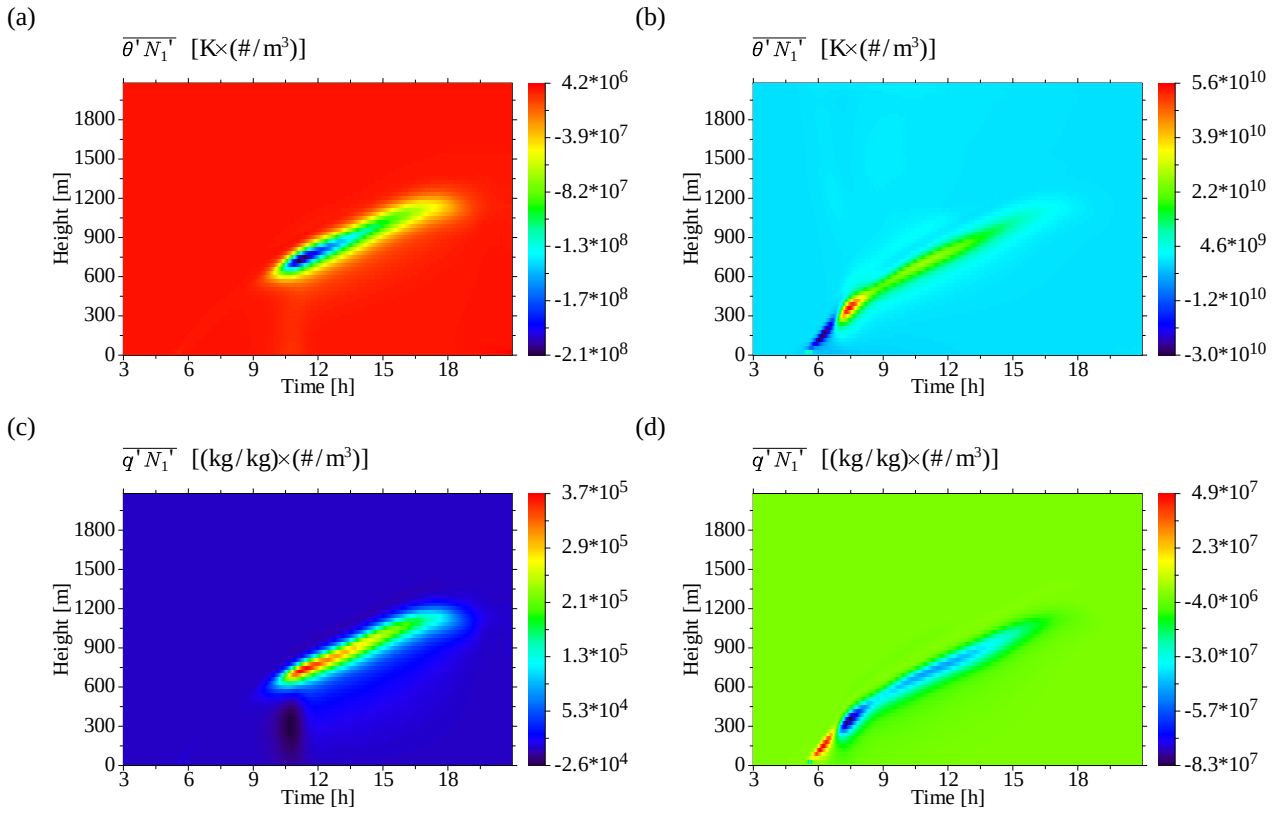

Fig. 8. Co-variances of meteorological parameters and physicochemical properties: **(a)** Co-variance of potential temperature and UCN number concentration – binary case; **(b)** Co-variance of potential temperature and UCN number concentration – ternary case; **(c)** Co-variance of water vapour mixing ratio and UCN number concentration – binary case; **(d)** Co-variance of water vapour mixing ratio and UCN number concentration – ternary case.

tropospheric air depleted from total NH_3 and UCNs into the CBL ($\overline{NH_{3,tot}' N_1'} > 0$). The positive correlation sets firstly in, when new particles were formed. The same happens also for the ternary case, but here the strongest positive correlation already occurs in the early morning, when the MLH is very low and the concentration of total NH_3 from surface emission sources is relatively high.

$\overline{H_2SO_4' N_1'}$ (Figs. 9c, d): As for the antecedent correlation pair, the cross-correlations of H_2SO_4 vapour and UCN number concentration for the binary and ternary case strongly differ. In the binary case, we have $\overline{H_2SO_4' N_1'} > 0$ with a pronounced maximum in the forenoon just below the MLH (Fig. 9c), where binary NPF occurs (Figs. 4a, c). To enable nucleation to occur, the H_2SO_4 vapour concentration must exceed a certain threshold (Fig. 3e). The positive correlation between H_2SO_4 vapour and UCN number concentration shows the entrainment of UCN-poor and H_2SO_4 vapour-poor free-tropospheric air into the CBL and/or detrainment of UCN-enriched and H_2SO_4 vapour-enriched CBL air into the free troposphere. In the ternary case, the $\overline{H_2SO_4' N_1'}$ correlation presented in Fig. 9d corresponds well to the pattern shown in Fig. 9b. The UCNs formed in situ in the surface layer in the early morning are positively correlated with the H_2SO_4 vapour, starting to form from photooxidation of SO_2 and OH. At that time, the SO_2 concentration, originating from surface emissions, is enhanced due to the low MLH. Even if the OH concentration is still low, H_2SO_4 vapour starts to form and fill the CBL reservoir until NPF sets in. Hence, $\overline{H_2SO_4' N_1'} > 0$ occurring in the early morning indicates turbulence-induced entrainment of H_2SO_4 vapour-poor and UCN-poor residual layer air into the growing CBL and/or detrainment of H_2SO_4 vapour-enriched and UCN-enriched CBL air into the residual layer.

5.3 Physicochemical variables in the surface layer

The time series of physicochemical variables in the surface layer are shown in Figs. 10 to 12.

The evolution of gas phase species near the surface is depicted in Fig. 10a. The temporal development of SO_2 and total NH_3 is controlled by the interplay between emission and dilution. Owing to its larger emission strength, the concentration of SO_2 is always higher than that of total NH_3. In the morning hours, the corresponding concentrations are enhanced due to emission into the surface layer with weak tur-

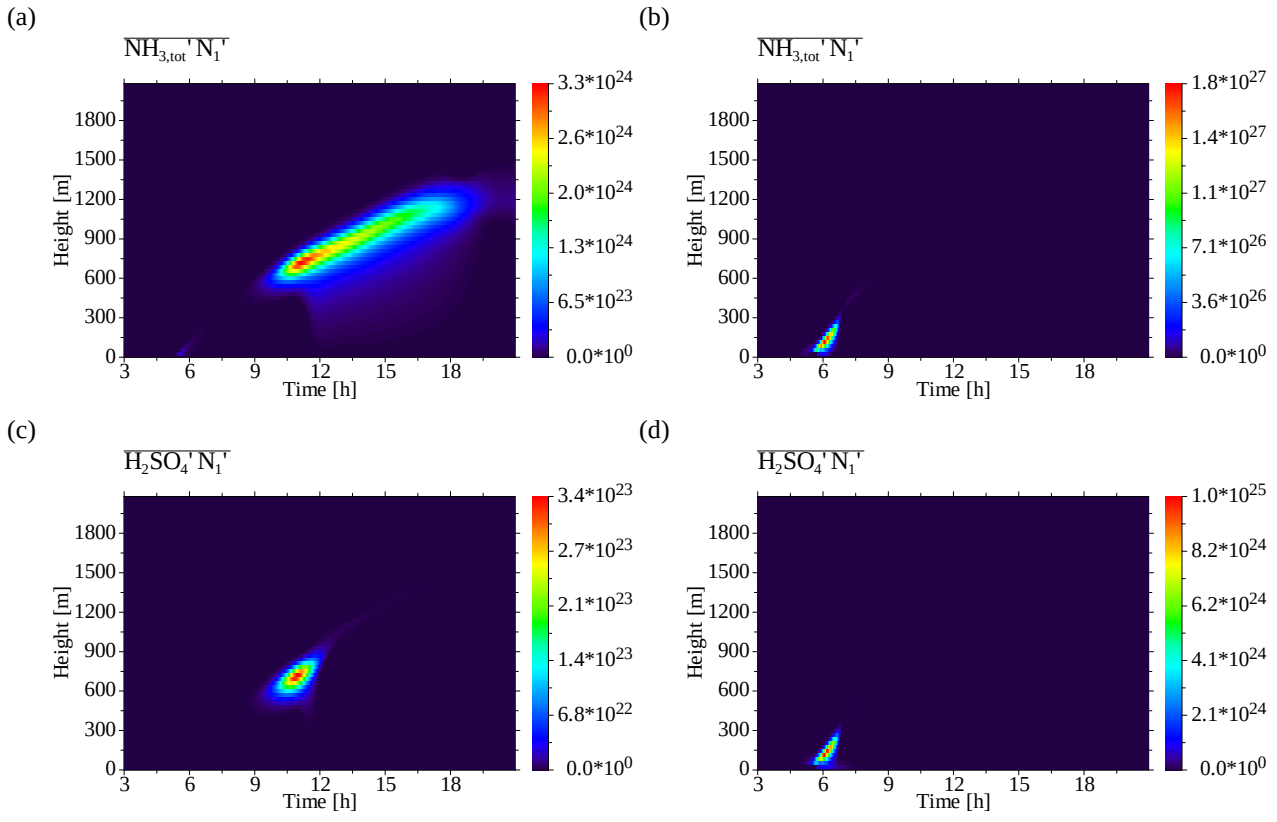

Fig. 9. Co-variances of gas phase concentrations and UCN number concentration: **(a)** Co-variance of total NH_3 concentration and UCN number concentration – binary case; **(b)** Co-variance of total NH_3 concentration and UCN number concentration – ternary case; **(c)** Co-variance of H_2SO_4 concentration and UCN number concentration – binary case; **(d)** Co-variance of H_2SO_4 concentration and UCN number concentration – ternary case.

bulence. In the course of the day, the concentrations decrease owing to turbulence-induced dilution. In the evening, when the mixed layer collapses, concentrations increase again. The gas phase concentration of NH_3, obtained from the equilibrium aerosol model, follows strongly the evolution of total NH_3. The NH_3 gas phase concentration is by several orders of magnitude lower than the total NH_3 concentration. The OH concentration from the semi-empirical model follows the solar elevation, i.e., reaching its maximum around noon. The H_2SO_4 vapour concentration is closely correlated to the concentration of OH. For the ternary case, H_2SO_4 vapour concentration is lower due to higher condensation sink, resulting from the higher UCN number concentration.

In Fig. 10b, the relative humidity and relative acidity are shown. The relative humidity peaks in the morning and evening hours, mainly controlled by the temperature evolution. In the course of the day, the relative humidity decreases due to turbulent mixing and solar-induced warming. The evolution of the relative acidity corresponds well to the H_2SO_4 vapour concentration in Fig. 10a. Due to the temperature dependency, the relative acidity strongly decreases during the day. In the ternary case, the relative acidity is much lower owing to the higher condensation sink.

Figure 10c shows the time series of the nucleation rate in the surface layer. The ternary nucleation rate is a few orders of magnitude higher than the binary one. The cut-off at $J_{nuc}=10^{-5}\,cm^{-3}\,s^{-1}$ denotes the limits of the validity of the parameterisation (Napari et al., 2002b). While the ternary nucleation rate gives a signal of in situ NPF in the morning hours, the binary one does not ($J_{nuc}<10^{0}\,cm^{-3}\,s^{-1}$).

Figure 11 shows the time series of the number and mass concentration of UCN mode, Aitken mode and accumulation mode particles. In connection with the corresponding time-height cross-sections, the typical evolution pattern of the UCN number concentration in Fig. 11a allows us to deduce the origin of UCNs observable in the surface layer. The ternary case pattern reveals a pronounced burst in the early morning, when the ternary nucleation rate (Fig. 10c) peaks. Afterwards, the UCN number concentration decreases due to intra-mode and inter-mode coagulation. The lack of a subsequent peak, when turbulence becomes important, points to in situ, i.e., local NPF, controlled by enhanced NH_3 concentration in the morning surface layer. In opposite to this, the binary case pattern reveals a pronounced,

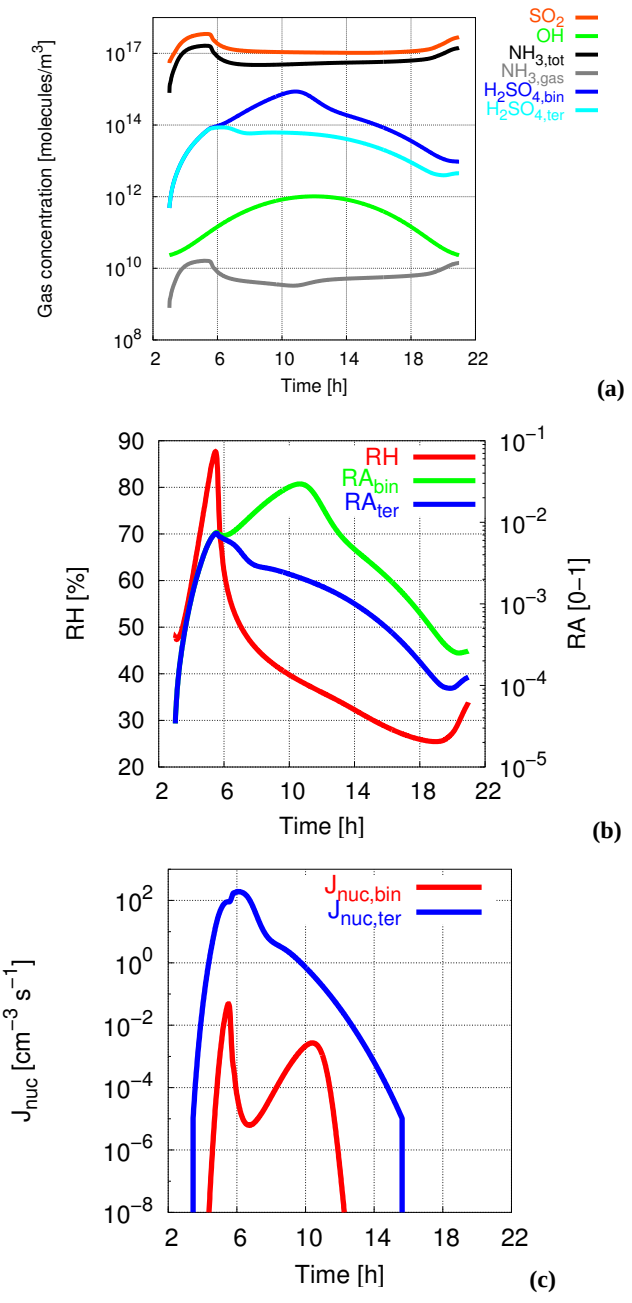

Fig. 10. Time series of physicochemical properties in the surface layer: **(a)** Gas phase species; **(b)** Relative humidity and relative acidity; **(c)** Nucleation rate.

but much lower burst at a time, when the binary nucleation rate in the surface layer is subcritical but CBL turbulence becomes important. This pattern points to ex situ, i.e., non-local NPF in the upper parts of the CBL, followed by turbulent downward transport of UCNs. The antecedent secondary peak in the morning hours is formed in situ due to temporally enhanced relative humidity and relative acidity as well as due to low temperature. But this secondary peak is by two orders of magnitude lower than the subsequent primary peak. The differences in the evolution of the UCN mass concentration seen in Fig. 11b result from the different burst patterns and from different condensation growth. In the ternary case, UCNs are formed at a much earlier time, hence starting earlier to consume H_2SO_4 vapour for particle growth by condensation. In opposite to this, in the binary case the bulk of UCNs is formed at a later time at a much lower rate. However, due to the higher H_2SO_4 concentration in the binary case, the condensation growth proceeds at a higher rate. Hence, the lower binary UCN production is overcompensated by an enhanced condensation growth, which leads to nearly the same UCN mass concentration around noon in both scenarios. The evolution of number concentration of Aitken mode and accumulation mode particles in Figs. 11c, e can be explained by the interplay of deposition, entrainment as well as intra-mode and inter-mode coagulation. The initial night-time value of the pre-existing Aitken mode number concentration is very low (Fig. 11c). It strongly decreases due to the dominant effect of dry deposition. When the CBL starts to grow, the Aitken mode particles are entrained from above into the surface layer, leading to a jump in the time series of number concentration in the early morning. The further evolution is controlled by intra-mode and inter-mode coagulation loss, deposition and turbulent mixing. In the binary case, the decrease of Aitken mode number concentration is weaker than in the ternary case due to a somewhat lower coagulation rate. The coagulation rate depends on the particle radius, that is diagnostically determined from mass and number concentration. The time series of the accumulation mode number concentration for the binary and ternary case, shown in Fig. 11e, are quite similar. They are also controlled by intra-mode and inter-mode coagulation loss, deposition and turbulent mixing. The differences in the evolution of the Aitken mode and the accumulation mode mass concentration between the binary and ternary case (cf. Figs. 11d, f) originate from the competition of the condensation growth in these two modes with that in the UCN mode. In the ternary case, the early start of NPF and subsequent condensation growth of UCNs (Fig. 11b) reduces the H_2SO_4 vapour amount, that is available for further growth and mass accumulation of pre-existing particles. Considering the different scales in Figs. 11b, d, f one can see, that the mass concentration of accumulation mode particles in Fig. 11f undergoes a weak jump in the time series in the morning.

Figure 12 shows the turbulent vertical fluxes of the UCN number concentration in the surface layer for the binary and the ternary case. In each case, a pronounced peak of the downward directed UCN flux appears, which coincides with a primary NPF burst. In the binary case, the downward UCN flux maximum at forenoon coincides with the “blob”-like NPF evolution pattern, appearing in Figs. 4a, c. This downward UCN flux maximum corresponds well to the time-height cross-section of the UCN flux in Fig. 6e. Analogous

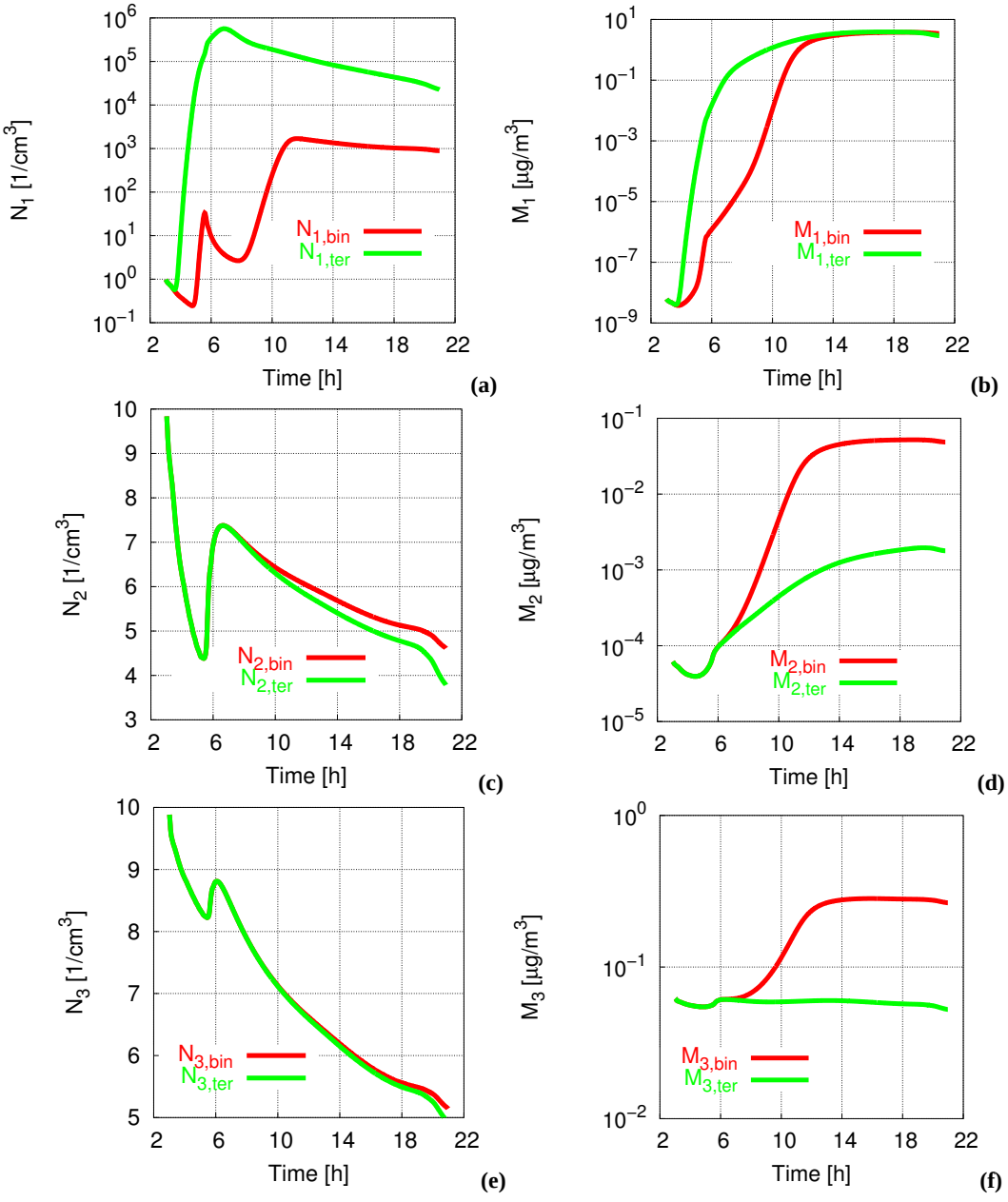

Fig. 11. Time series of physicochemical properties in the surface layer: **(a)** Nucleation mode number concentration; **(b)** Nucleation mode mass concentration; **(c)** Aitken mode number concentration; **(d)** Aitken mode mass concentration; **(e)** Accumulation mode number concentration; **(f)** Accumulation mode mass concentration.

in the ternary case, there is a coincidence of the maximum of downward UCN flux with the "sucking tube"-like NPF evolution pattern, depicted in Figs. 4b, d, which also corresponds well to the time-height cross-section of the UCN flux in Fig. 6f.

6 Summary and conclusion

The model approach presented here is suitable to simulate selected aspects regarding the contribution of turbulence to the spatio-temporal occurrence of NPF bursts in the CBL. The intercomparison of synthetic scenarios of binary and ternary NPF in the anthropogenically influenced CBL, using state-of-the-art nucleation models, reveals large differences in the evolution of the UCN number concen-

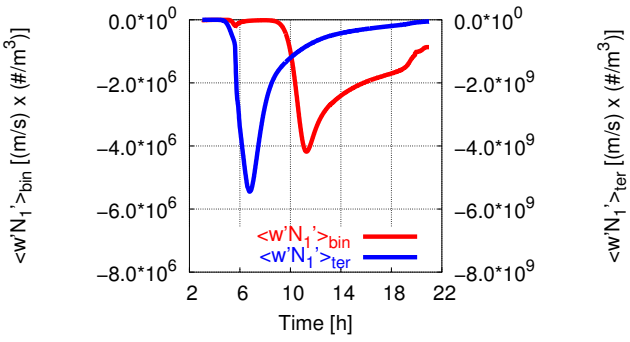

Fig. 12. Time series of physicochemical properties in the surface layer: Turbulent vertical flux of UCNs for binary and ternary nucleation.

tration in the surface layer as well as in the time-height cross-sections of first-order moments and double correlation terms. Although in both cases the occurrence of NPF bursts could be simulated, the burst characteristics and genesis are completely different. It was demonstrated, that observations from the surface layer alone are not conclusive to elucidate the origin of newly formed particles. This is also true with respect to the interpretation of box modelling studies.

The binary and ternary NPF bursts, predicted to occur in the surface layer, differ with respect to burst amplitude and phase. In the considered binary scenario, the burst evolution is a direct result of the interaction of photochemically produced H_2SO_4 vapour and CBL turbulence. New particles are formed in the forenoon in the upper part of the growing CBL, followed by turbulence-induced top-down transport. Hence, with respect to the burst observation site in the surface layer, new particles are formed ex situ. In opposite to this, the ternary case reveals a much more complex pattern. Here, NPF is much less controlled by H_2SO_4 vapour. NPF is initiated in the early morning hours in the surface layer, when temperature is low and SO_2 and NH_3 concentrations are high, hence UCNs are formed in situ. The damping effect of the low H_2SO_4 concentration onto the nucleation rate at that time is overcompensated by the forcing effect of the enhanced NH_3 concentration. Shortly after that, ex situ NPF in the free troposphere sets in, followed by entrainment and top-down diffusion of newly formed particles toward the surface layer. The strong ternary nucleation signal at the top of the model domain is mainly related to the quite low relative humidity there. Altogether, these processes contribute to the formation of a strong burst in the morning hours. The ternary case simulation shows, that NH_3 not only serves as a constant offset or tuning parameter in nucleation models, but undergoes a diurnal evolution strongly controlled by CBL turbulence. Hence, its impact on the burst evolution is non-linear. While the time-height cross-section of the binary nucleation rate resembles a "blob"-like evolution pattern, the ternary one resembles a "sucking tube"-like pattern. The time-height cross-sections of the flux patterns and double correlations could be plausibly interpreted in terms of CBL turbulence and entrainment/detrainment processes, both in the binary and ternary case.

The simulations provide a number of predictive high-order moments, that can not yet be directly verified by observations. However, these fields behave reasonably and provide an insight from a modelling point of view into the genesis and special conditions, under which NPF was hypothesised to occur in the boundary layer. The considered synthetic scenarios do not represent climatologically typical CBL conditions, especially with respect to the low aerosol background concentrations, leading to H_2SO_4 concentrations, which are too high compared to previous observations. This results in an overestimation of the nucleation rate, especially in the binary scenario. Moreover, the scenarios are restricted to classical homogeneous nucleation involving only up to three species (water vapour, H_2SO_4 vapour, NH_3). Condensation growth by organic vapours is not considered. Even though not typical, the assumed scenarios of an anthropogenic emission source in a post-frontal clean air mass are at least instructive to elucidate the interactions between CBL turbulence, SO_2 and NH_3 chemistry as well as aerosol dynamics by means of a self-consistent turbulence modelling approach. Apart from a comprehensive model verification/validation study, further scenario simulations are necessary to systematically verify or falsify, respectively, the number of state-of-the-art hypothesis on NPF currently under discussion. Also, a more advanced description of the formation and activation of thermodynamically stable clusters in the model is deserved, such as proposed by Kulmala et al. (2000), Kulmala (2003) and Kulmala et al. (2004a, 2006). In the subsequent Paper IV an attempt is made to re-evaluate previous observations of NPF in the CBL with respect to the two scenarios investigated here.

Acknowledgements. The work was realised at the IfT Modelling Department headed by E. Renner within the framework of IfT main research direction 1 "Evolution, transport and spatio-temporal distribution of the tropospheric aerosol". For the motivation and numerous discussions on the subject of the present Paper I am very indebted to D. Mironov, E. Renner, K. Bernhardt, E. Schaller, M. Kulmala, A. A. Lushnikov, M. Boy, R. Wolke, F. Stratmann, H. Siebert, T. Berndt and J. W. P. Schmelzer. Sincerest thanks are given to M. Kulmala and M. Boy for the opportunity to present and discuss previous results at the Department of Physics at the University of Helsinki as well as to J. W. P. Schmelzer for the chance to discuss selected aspects of cluster formation under atmospheric conditions, generalisation of classical Gibbs theory and phase transformations in multicomponent systems during the X^{th} Research Workshop on Nucleation Theory and Applications at the Bogoliubov Laboratory of Theoretical Physics of the Joint Institute for Nuclear Research (JINR), Dubna. In this context, I want to express special thanks also to A. K. Shchekin, A. S. Abyzov, H. Heinrich and I. S. Gutzow. Many thanks go to the editor

and to the three reviewers for their helpful comments, additional references and suggestions to improve the manuscript. Special thanks go also to N. Otto and N. Deisel for their strong support during the technical processing as well as to M. Reichelt for the proofreading of the manuscript.

Edited by: M. Kulmala

References

Birmili, W., Wiedensohler, A., Plass-Dülmer, C., and Berresheim, H.: Evolution of newly formed aerosol particles in the continental boundary layer: A case study including OH and H_2SO_4 measurements, Geophys. Res. Lett., 27(15), 2205–2208, 2000.

Birmili, W., Berresheim, H., Plass-Dülmer, C., Elste, T., Gilge, S., Wiedensohler, A., and Uhrner, U.: The Hohenpeissenberg aerosol formation experiment (HAFEX): A long-term study including size-resolved aerosol, H_2SO_4, OH, and monoterpenes measurements, Atmos. Chem. Phys., 3, 361–376, 2003, http://www.atmos-chem-phys.net/3/361/2003/.

Boy, M., Kulmala, M., Ruuskanen, T. M., Pihlatie, M., Reissell, A., Aalto, P. P., Keronen, P., Dal Maso, M., Hellen, H., Hakola, H., Jansson, R., Hanke, M., and Arnold, F.: Sulphuric acid closure and contribution to nucleation mode particle growth, Atmos. Chem. Phys., 5, 863–878, 2005, http://www.atmos-chem-phys.net/5/863/2005/.

Jaecker-Voirol, A. and Mirabel, P.: Nucleation rate in a binary mixture of sulfuric acid and water vapor, J. Phys. Chem., 92, 3518–3521, 1988.

Jaecker-Voirol, A. and Mirabel, P.: Heteromolecular nucleation in the sulfuric acid–water system, Atmos. Environ., 23, 2053–2057, 1989.

Jaecker-Voirol, A., Mirabel, P., and Reiss, H.: Hydrates in supersaturated binary sulfuric acid–water vapor: A reexamination, J. Chem. Phys., 87, 4849–4852, 1987.

Korhonen, P., Kulmala, M., Laaksonen, A., Viisanen, Y., McGraw, R., and Seinfeld, J. H.: Ternary nucleation of H_2SO_4, NH_3, and H_2O in the atmosphere, J. Geophys. Res., 104(D21), 26 349–26 353, 1999.

Kulmala, M.: How particles nucleate and grow, Science, 302, 1000–1001, 2003.

Kulmala, M. and Laaksonen, A.: Binary nucleation of water–sulfuric acid system: Comparison of classical theories with different H_2SO_4 saturation vapor pressures, J. Chem. Phys., 93, 696–701, 1990.

Kulmala, M., Laaksonen, A., and Pirjola, L.: Parameterizations for sulfuric acid/ water nucleation rates, J. Geophys. Res., 103(D7), 8301–8307, 1998.

Kulmala, M., Pirjola, L., and Mäkelä, J. M.: Stable sulphate clusters as a source a new atmospheric particles, Nature, 404, 66–69, 2000.

Kulmala, M., Kerminen, V.-M., Anttila, T., Laaksonen, A., and O'Dowd, C. D.: Organic aerosol formation via sulphate cluster activation, J. Geophys. Res., 109, D04205, doi:10.1029/2003JD003961, 2004a.

Kulmala, M., Vehkamäki, H., Petäjä, T., Dal Maso, M., Lauri, A., Kerminen, V.-M., Birmili, W., and McMurry, P. H.: Formation and growth rates of ultrafine atmospheric particles: A review of observations, J. Aerosol Sci., 35, 143–176, 2004b.

Kulmala, M., Lehtinen, K. E. J., and Laaksonen, A.: Cluster activation theory as an explanation of the linear dependence between formation rate of 3 nm particles and sulphuric acid concentration, Atmos. Chem. Phys., 6, 787–793, 2006, http://www.atmos-chem-phys.net/6/787/2006/.

Laaksonen, A. and Kulmala, M.: Homogeneous heteromolecular nucleation of sulphuric acid and water vapours in stratospheric conditions: A theoretical study of the effect of hydrate interaction, J. Aerosol Sci., 22, 779–787, 1991.

Liu, X., Hegg, D. A., and Stoelinga, M. T.: Numerical simulation of new particle formation over the northwest Atlantic using the MM5 mesoscale model coupled with sulfur chemistry, J. Geophys. Res., 106(D9), 9697–9715, 2001.

Napari, I., Noppel, M., Vehkamäki, H., and Kulmala, M.: An improved model for ternary nucleation of sulfuric acid-ammonia-water, J. Chem. Phys., 116, 4221–4227, 2002a.

Napari, I., Noppel, M., Vehkamäki, H., and Kulmala, M.: Parametrization of ternary nucleation rates for H_2SO_4–NH_3–H_2O vapors, J. Geophys. Res., 107(D19), 4381, doi:10.1029/2002JD002132, 2002b.

Pirjola, L. and Kulmala, M.: Modelling the formation of H_2SO_4–H_2O particles in rural, urban and marine marine conditions, Atmos. Res., 46, 321–347, 1998.

Seinfeld, J. H. and Pandis, S. N.: Atmospheric Chemistry and Physics. From Air Pollution to Climate Change, John Wiley & Sons, Inc., New York, 1998.

Stauffer, D.: Kinetic theory of two-component ("heteromolecular") nucleation and condensation, J. Aerosol Sci., 7, 319–333, 1976.

Verver, G. H. L., van Dop, H., and Holtslag, A. A. M.: Turbulent mixing of reactive gases in the convective boundary layer, Boundary-Layer Meteorol., 85, 197–222, 1997.

Weber, R. J., Marti, J. J., McMurry, P. H., Eisele, F. L., Tanner, D. J., and Jefferson, A.: Measured atmospheric new particle formation rates: Implications for nucleation mechanisms, Chem. Eng. Comm., 151, 53–64, 1996.